mathematics

MDPI

Article

Modified Remora Optimization Algorithm for Global Optimization and Multilevel Thresholding Image Segmentation

Qingxin Liu [1], Ni Li [2,3], Heming Jia [4,*], Qi Qi [1,*] and Laith Abualigah [5,6]

1 School of Computer Science and Technology, Hainan University, Haikou 570228, China; qxliu@hainanu.edu.cn
2 School of Mathematics and Statistics, Hainan Normal University, Haikou 571158, China; lini@hainnu.edu.cn
3 Key Laboratory of Data Science and Intelligence Education of Ministry of Education, Hainan Normal University, Haikou 571158, China
4 School of Information Engineering, Sanming University, Sanming 365004, China
5 Faculty of Computer Sciences and Informatics, Amman Arab University, Amman 11953, Jordan; aligah.2020@gmail.com
6 School of Computer Science, Universiti Sains Malaysia, Pulau Pinang 11800, Malaysia
* Correspondence: jiaheming@fjsmu.edu.cn (H.J.); qqi@hainanu.edu.cn (Q.Q.)

Abstract: Image segmentation is a key stage in image processing because it simplifies the representation of the image and facilitates subsequent analysis. The multi-level thresholding image segmentation technique is considered one of the most popular methods because it is efficient and straightforward. Many relative works use meta-heuristic algorithms (MAs) to determine threshold values, but they have issues such as poor convergence accuracy and stagnation into local optimal solutions. Therefore, to alleviate these shortcomings, in this paper, we present a modified remora optimization algorithm (MROA) for global optimization and image segmentation tasks. We used Brownian motion to promote the exploration ability of ROA and provide a greater opportunity to find the optimal solution. Second, lens opposition-based learning is introduced to enhance the ability of search agents to jump out of the local optimal solution. To substantiate the performance of MROA, we first used 23 benchmark functions to evaluate the performance. We compared it with seven well-known algorithms regarding optimization accuracy, convergence speed, and significant difference. Subsequently, we tested the segmentation quality of MORA on eight grayscale images with cross-entropy as the objective function. The experimental metrics include peak signal-to-noise ratio (*PSNR*), structure similarity (*SSIM*), and feature similarity (*FSIM*). A series of experimental results have proved that the MROA has significant advantages among the compared algorithms. Consequently, the proposed MROA is a promising method for global optimization problems and image segmentation.

Keywords: remora optimization algorithm; multi-level thresholding image segmentation; cross-entropy; meta-heuristic; optimization

MSC: 65Y04; 68Q25

Citation: Liu, Q.; Li, N.; Jia, H.; Qi, Q.; Abualigah, L. Modified Remora Optimization Algorithm for Global Optimization and Multilevel Thresholding Image Segmentation. *Mathematics* **2022**, *10*, 1014. https://doi.org/10.3390/math10071014

Academic Editors: Alma Y. Alanis and Mihai Postolache

Received: 9 February 2022
Accepted: 18 March 2022
Published: 22 March 2022

1. Introduction

Image segmentation technique is a primary step in computer vision and pattern recognition for pre-processing and analyzing images in the fields of remote sensing, medicine, etc. [1–5]. This technique divides an image into several homogeneous regions or segments with similar characteristics according to features, color, texture, and contrast [6,7]. In the literature, there exist four common types of image segmentation techniques, which can be categorized into (1) region-based techniques, (2) graph-based techniques, (3) clustering-based techniques, and (4) thresholding-based techniques [8]. Among them, the thresholding-based method has gained more attention from researchers due to its efficiency and ease of

implementation. The thresholding-based technique can be categorized into bi-level and multi-level thresholding [9]. As the name suggests, the bi-level thresholding uses a single threshold value to segment an image into two homogeneous foreground and background areas. By contrast, multi-level thresholding divides an image into more than two regions based on pixel intensities [10–12]. Thus, the multi-level thresholding technique has widely applied in various fields by researchers. However, selecting suitable threshold values is still the most challenging problem and requires further research.

To determine optimal threshold values to segment a given image into several regions, there are two approaches commonly used, which are Otsu's method (by maximizing between-class variance) and Kapur's entropy (by maximizing the entropy of the classes) [13]. These methods are suitable for determining a single threshold value. However, when extended into multi-level thresholding, the fatal shortcomings are the computational time and complexity. Therefore, various nature-inspired MAs were proposed in the literature to handle these problems and gained excellent performance [14–16].

MAs are considered stochastic algorithms that use randomly generated search agents and specific operators to determine optimal solutions in the search space instead of gradient information. These operators are inspired by nature, such as swarm behavior, social behavior, physics, evolutionary rules, etc. [17–25]. Over the last years, various MAs have been proposed and applied in complex real-world problems. Such MAs can be categorized into three main categories: (1) swarm intelligence-based methods, (2) nature evolution-based methods, (3) physics-based methods. The first category mainly simulates the swarm behavior of biological entities, such as birds, slime mould, or the grey wolf. Particle Swarm Optimization (PSO) [26] is one of the most popular MAs inspired by the foraging behavior of birds. Grey Wolf Optimizer (GWO) [27] simulates the grey wolf's hunting behavior and leadership relationship. Slime Mould Algorithm (SMA) [28] imitates the slime mould's contraction and oscillation mode during foraging. Other popular MAs in the first category include the Whale Optimization Algorithm (WOA) [29], Cuckoo Search Algorithm (CSA) [30], Salp Swarm Algorithm (SSA) [31], Ant Colony Optimization (ACO) [32], Harris Hawks Optimization (HHO) [33], Moth Flame Optimization (MFO) [34], and Aquila Optimizer (AO) [35]. The second category mainly imitates the evolution process in nature. Genetic Algorithm (GA) [36] is the most famous one developed by the Darwinian evolution law. Some other popular algorithms include Evolutionary Strategy (ES) [37], Differential Evolution (DE) [38], Genetic Programming (GP) [39], Bio-geography-Based Optimizer (BBO) [40], and Evolution Strategy (ES) [41]. The physics-based method simulates the physical laws of the universe. One of the most popular algorithms in this category is Simulated Annealing (SA) [42], which mimics the principle of simulated annealing. It starts from a higher initial temperature, then reduces with the decrease in temperature parameters. Established by this principle, other algorithms include Gravity Search Algorithm (GSA) [43], Gradient-based method (GBO) [44], Sine Cosine Algorithm (SCA) [45], Golden Sine Algorithm (Gold-SA) [46], Arithmetic Optimization Algorithm (AOA) [47], Henry Gas Solubility Optimization (HGSO) [48], Atom Search Optimization (ASO) [49], Central Force Optimization (CFO) [50], and Multi-Verse Optimizer (MVO) [51]. Although many nature-inspired MAs were proposed to solve numerical optimization problems, as real-world problems grow in complexity and difficulty, we need to present more useful MAs to handle them.

Jia et al. [52] presented a new nature-inspired meta-heuristic, namely the Remora Optimization Algorithm (ROA). The main inspiration of ROA is the parasitic behavior of remora during foraging in the ocean. ROA integrates different position update rules based on different hosts. As one of the intelligent creatures in the world, remora usually adsorbs on different hosts to achieve movement and foraging, so the location update rules are the same as those of the host. Moreover, remora also attempt to move by themselves, which is used to determine whether to change hosts. The experimental results demonstrated that the ROA is superior to other algorithms in terms of optimization accuracy and convergence speed. Zheng et al. [53] proposed an improved ROA, namely IROA, for solving global

optimization problems. In this work, a mechanism called autonomous foraging was proposed. This mechanism allows each remora a small chance to find the food randomly or according to the current food position, which was used to improve the ROA's optimization accuracy. Then, the IROA's performance was evaluated on function optimization and five constrained engineering design problems. The experimental results demonstrated that IROA has a superior performance to other selected MAs in terms of optimization accuracy and convergence speed. However, the No-Free-Lunch (NFL) theorem [54] stated that no unique MAs are available to solve any optimization problems, which encourages us to develop more efficient methods and apply them in various fields such as multi-level thresholding problems.

This paper presents a modified Remora Optimization Algorithm called MROA for global optimization and multi-level thresholding image segmentation tasks. The motivations of this work are to alleviate ROA's weaknesses and enhance its performance in solving image segmentation tasks. The two major improvements are contained in this work. First, Brownian motion is used to enhance the ROA's exploration ability and provide it with a high level of opportunity to find the optimal or near-optimal solution in the search space. Second, the lens opposition-based learning strategy is used to improve the exploitation ability of ROA and help search agents to jump out the local optimal solution. We first used 23 benchmark functions in the experimental design including unimodal and multimodal types to validate its performance.

Furthermore, we selected eight grayscale images as the benchmark images, and cross-entropy is employed as the objective function to evaluate the segmentation quality of search agents. We compared MROA with other well-known algorithms and its original in all the tests such as ROA, RSA, AOA, AO, SSA, SCA, and GWO. The experimental results reveal that MROA significantly improved compared with these others in segmentation precision and convergence speed. Overall, it can be proved that MROA is an effective method for global optimization and multi-level thresholding.

The main contributions of this paper can be summarized as follows:

- A new modified ROA, namely MROA, is first proposed based on BM and LOBL strategies.
- The optimization performance of the MROA is evaluated on 23 benchmark functions.
- MROA is applied for thresholding segmentation using the cross-entropy method.
- Validate segmentation quality of MROA in terms of *PSNR*, *SSIM*, *FSIM*, and statistical test.
- The performance of MROA is compared with seven well-known MAs.

The rest of this paper is organized as follows. Section 2 introduces the related work of multi-level thresholding image segmentation using MAs. Section 3 briefly describes the background knowledge. Section 4 presents the proposed MROA. The experimental results are introduced and analyzed in Sections 5 and 6. Finally, Section 7 concludes this paper and gives future research directions.

2. Related Works

The MAs-based multi-level thresholding segmentation technique has gained more attention from scholars because of its reliable performance, small computational cost, and ease of implementation. In this field, determining the threshold values is the core of the entire segmentation process in the multi-level thresholding technique. In many application scenarios, many scholars use the exhaustive method to determine the optimal threshold values. However, this method has fatal disadvantages, such as complexity, time-consuming computation, and poor threshold values. Therefore, to alleviate these shortcomings, many works show the efficiency and performance of MAs in obtaining optimal threshold values; the following are a few outstanding research works. In [55], Jia et al. presented an efficient satellite image segmentation approach, called DHHO/M, based on dynamic HHO with a mutation mechanism. This work introduces the dynamic control parameter mechanism and mutation operators to improve HHO performance and avoid falling into local optimal solutions. Kapur's entropy, Otsu between-class variance, and Tsallis entropy

were employed to determine optimal threshold values. In the experiments, eight color satellite images and four oil pollution images validate DHHO/M's performance. The experimental results demonstrated that the DHHO/M provided competitive performance in fitness evaluation, segmentation quality, and statistical tests compared with eight advanced thresholding techniques.

Ewees et al. [56] proposed a new multi-level thresholding method, using modified artificial ecosystem-based optimization (AEO), namely AEODE. The AEODE integrated differential evolution as a local search operator to overcome AEO's shortcomings. In this way, the AEODE was used to determine a set of optimal threshold values and fuzzy entropy as the objective function. Then, the AEODE was accessed by different grayscale images at six various threshold values. The experimental results show that AEODE outperforms others, including original AEO and DE, in terms of fitness values, *PSNR*, *SSIM*, and *FSIM*.

In [57], an improved version of MPA with an opposition-based learning strategy called MPA-OBL was proposed to determine optimal threshold values at different thresholds. The Otsu between-class variance and Kapur's were employed as the objective function in this work. The proposed method was evaluated on CEC 2020 test suite and several benchmark images. Compared with ELSHADE-SPACMA-OBL, CMA-ES-OBL, DE-OBL, HHO-OBL, SCA-OBL, SSA-OBL, and standard MPA, the proposed technique MPA-OBL produced better results in different evaluation measurements.

Su et al. [58] presented a variant ABC, namely CCABC, which introduced vertical search and horizontal search mechanisms to improve ABC's optimization performance. Furthermore, the proposed method, CCABC, was used to find the appropriate threshold values in COVID-19 X-ray images based on Kapur's entropy. The proposed method was compared with a set of advanced and classical MAs. The evaluation results show that the CCABC is an excellent method in most quality measurements.

Liu et al. [59] proposed a novel multi-level thresholding segmentation technique based on a modified evolution algorithm, called MDE, and applied it to a breast cancer image segmentation task. In this work, the slime mold foraging behavior is introduced to enhance DE's optimization accuracy and convergence speed. Furthermore, three image quality metrics, including *PSNR*, *SSIM*, and *FSIM*, are used to evaluate its segmentation results to show its segmentation performance.

Li et al. [60] proposed a partitioned and cooperative quantum-behaved particle swarm optimization namely SCQPSO for processing stomach CT images. In this work, SCQPSO was used to determine the optimal threshold values according to Otsu's method. Additionally, the inter-class variance of Otsu and its variance was used to show SCQPSO's segmentation quality.

In the literature, we find that more and more scholars presented variants of the multi-level thresholding image segmentation method using MAs to determine optimal threshold values instead of the traditional exhaustive method. Consequently, we confirm that the meta-heuristic-based multi-level thresholding method is a promising work and interesting theories need further research. However, as real-world problems grow in complexity and difficulty, these methods will inevitably fail to find the optimal threshold values during segmentation. Therefore, image segmentation using MAs has more room for improvement to obtain better segmentation quality.

3. Background Knowledge

3.1. Remora Optimization Algorithm (ROA)

ROA [52] is a well-known bionics-based meta-heuristic algorithm inspired by the parasitic behavior of remora during foraging in the ocean. Unlike other fishes, remora usually attach to other hosts (humpback whales or sailfishes) to complete long and short-distance movement in the ocean. Like other MAs, ROA also has three different phases: initialization, exploration, and exploitation.

3.1.1. Initialization

Like other various meta-heuristic algorithms, ROA initializes the search agents using a random approach in the search space, which is calculated by:

$$X_i = lb + rand \times (ub - lb);\ i \in \{1, 2, \ \ldots\ , N\} \tag{1}$$

where *rand* denotes a random variable between [0, 1]. *ub* and *lb* indicate the search space's upper and lower bounds. *i* represents the number of Remora, and *N* denotes population size.

3.1.2. Free Travel (Exploration Phase)

ROA achieves long-distance and small global movements, respectively, in the search space based on the free travel method. This method includes two main sub-methods: SFO strategy and experience attack.

- SFO strategy

Sailfish: one of the fastest fish in the ocean. Thus, remora attaches to them to achieve quick long-distance movement, and its position update is the same as its host, which is calculated by:

$$X(t+1) = X_{best}(t) - (rand \times (\frac{X_{best}(t) + X_{rand}(t)}{2}) - X_{rand}(t)) \tag{2}$$

where $X_{best}(t)$ indicates global best position of remora and $X_{rand}(t)$ represents the random position.

- Experience attack

To determine whether the remora changes the host, it needs to take a small step around it. This activity is considered an experience attack and the formula is expressed by:

$$X_{att}(t+1) = X(t) + randn \times (X(t) - X_{pre}(t)) \tag{3}$$

where $X_{pre}(t)$ represents the position of the previous generation. *randn* indicates typically distributed random numbers between 0 to 1.

3.1.3. Eat Thoughtfully (Exploitation Phase)

- WOA strategy

When remora is attached to the humpback whale, its attack strategy is the same as the bubble-net attack strategy in WOA. The mathematical formula can be described as follows:

$$X(t+1) = D \times e^a \times \cos(2\pi\alpha) + X(t) \tag{4}$$

$$\alpha = rand \times (a - 1) + 1 \tag{5}$$

$$a = -(1 + \frac{t}{T}) \tag{6}$$

$$D = |X_{best}(t) - X(t)| \tag{7}$$

where *D* denotes the distance between the best position and current position. α is a random value between $[-1, 1]$.

- Host feeding

This method is a subdivision in the exploitation process. In this phase, remora moving around the host can be thought of as a small step, which can be calculated as follows:

$$X(t+1) = X(t) + A \tag{8}$$

$$A = B \times (X(t) - C \times X_{best}(t)) \tag{9}$$

$$B = 2 \times V \times rand - V \tag{10}$$

$$V = 2 \times (1 - \frac{t}{T}) \tag{11}$$

where A denotes a small step movement of remora, which is related to the volume of host and remora. A remora factor (C) is utilized to limit the position of remora to distinguish between the host and remora.

Figure 1 vividly illustrates the main process of ROA, and the pseudo-code of ROA is presented in Algorithm 1.

Algorithm 1 the pseudo-code of ROA

Inputs: N and T
Outputs: best solution
Initialize the positions of remora X_i (i = 1, 2, . . . , N);
While ($t \leq T$)
Check if any search agent goes beyond the search space and amend it;
Calculate the fitness of each remora;
For each remora indexed by i
H(i) = round(*rand*);
If H(i) == 0 **then**
Using Equation (4) to update the position of attached whales;
Elseif H(i) == 1 **then**
Using Equation (2) to update the position of attached sailfishes;
End if
Make a one-step prediction by experience attack (Equation (3));
If $f(X_{att}) < f(X)$ **then**
$X = X_{att}$;
H(i) = round(*rand*);
Else
Using Equation (8) to update the position of search agents;
End if
End for
End While

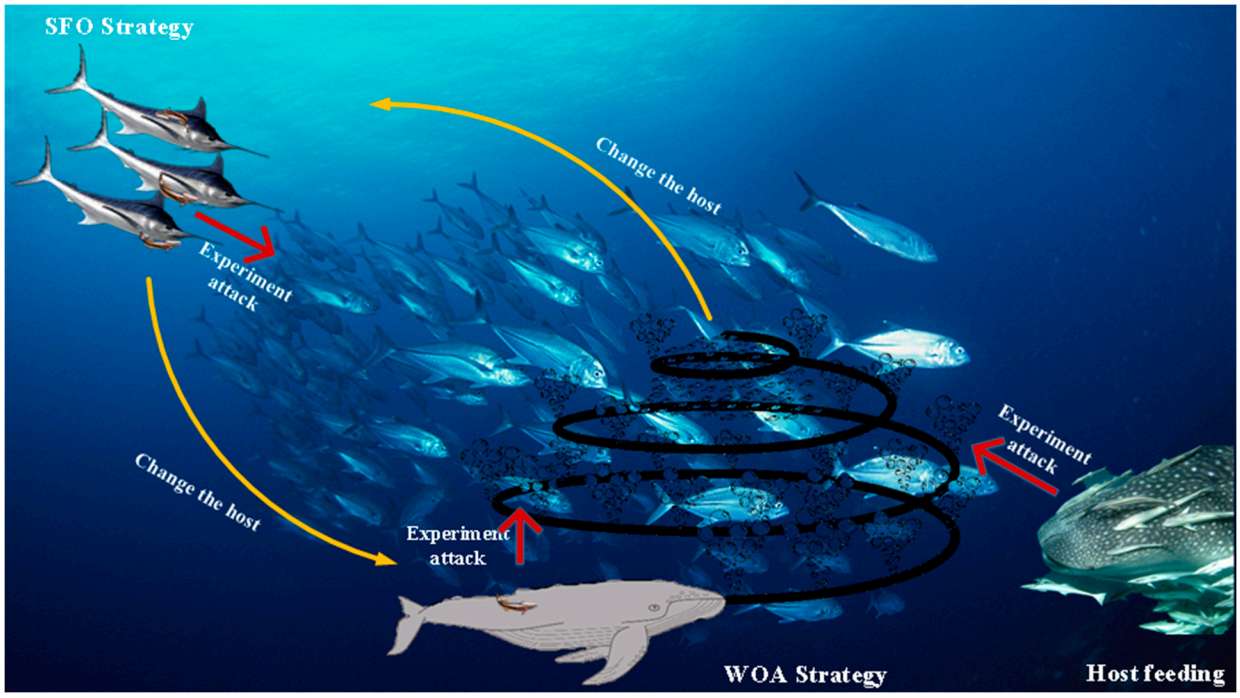

Figure 1. The different process of ROA.

3.2. Brownian Motion

Brownian motion (BM) is a stochastic process in which step length is drawn from the probability function defined by a normal distribution with zero mean ($\mu = 0$) and unit variance ($\sigma^2 = 1$) [61,62]. The probability density function at point x for BM is calculated via:

$$f_B(x;\mu,\sigma) = \frac{1}{\sqrt{2\pi\sigma^2}} \exp\left(-\frac{(x-\mu)^2}{2\sigma^2}\right) = \frac{1}{\sqrt{2\pi}} \exp\left(-\frac{x^2}{2}\right) \tag{12}$$

where x indicates a point following this motion and the distribution, 2D, and 3D trajectory of BM as shown in Figure 2. As the related figures show, we can see that BM can over areas of the domain with more uniform and controlled steps in the search space. On the other hand, BM's trajectory can trace and explore distant areas of the neighborhood.

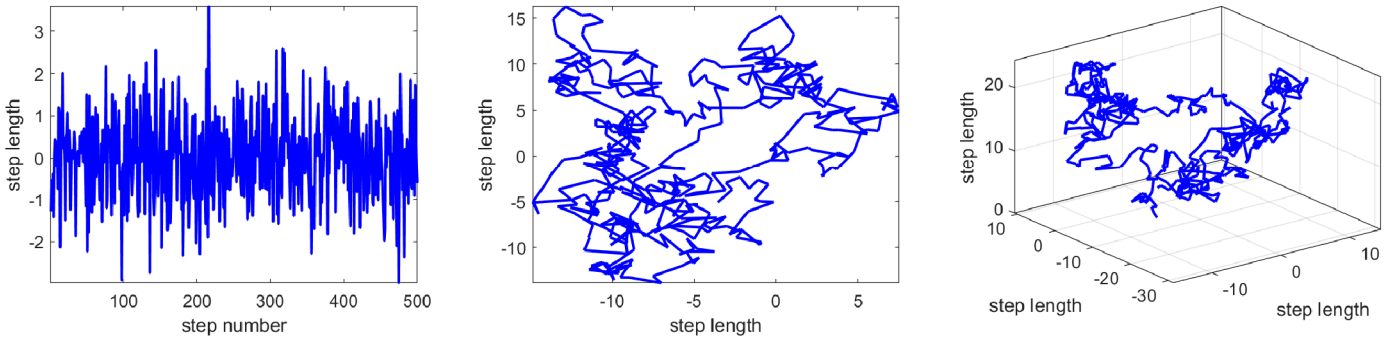

Figure 2. Brownian distribution, 2D Brownian trajectory, and 3D Brownian trajectory.

3.3. Lens Opposition-Based Learning

Lens opposition-based learning (LOBL) [63] is a novel strategy that integrates both opposition-based learning (OBL) [64] strategy and lens imaging principle to enhance the searchability of MAs. The LOBL strategy shows more effective performance during the

optimization process than OBL when finding optimal or near-optimal solutions in the search space. The mathematical principle of LOBL is described as follows:

Lens imaging theory illustrates that when the distance from the object to the lens exceeds two times the focal length, an inverted and constricted real image will be formed between 1–2 times the focal length on the other side of the lens. As shown in Figure 3, where O represents the midpoint of the interval [lb, ub] and the y-axis is treated as a convex lens. In addition, an object of height h is located at point x, which is twice the lens's focal length. Through lens imaging, the coordinates of the image vertices become (x^*, h^*). The formula is listed as follows:

$$\frac{(lb+ub)/2-x}{x^*-(lb+ub)/2}=\frac{h}{h^*} \tag{13}$$

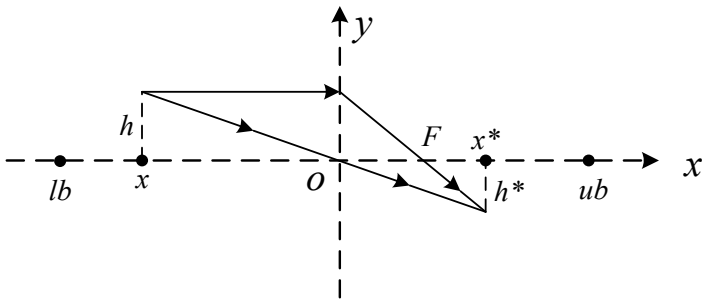

Figure 3. Diagram of LOBL.

Let $k = h/h^*$, Equation (14) can be simplified as follows:

$$x^*=\frac{lb+ub}{2}+\frac{lb+ub}{2k}-\frac{x}{k} \tag{14}$$

In general, the optimization tasks are multi-dimensional, so the Equation (15) can be extended as follows:

$$x_i{}^*=\frac{lb_i+ub_i}{2}+\frac{lb_i+ub_i}{2k}-\frac{x_i}{k} \tag{15}$$

where $x_i{}^*$ denotes the opposite point of x_i in i-th dimension. Interestingly, if $k = 1$, Equation (16) is the same as the OBL strategy. Therefore, the LOBL can be considered as a variant of OBL. The difference is that LOBL used an adjusting parameter k to realize dynamic search behavior when solving optimization tasks, which further improves the probability of the algorithm escaping from the local optimal solution.

3.4. Cross Entropy

In 1968, cross-entropy was proposed by Kullback [65]. As an essential concept in Shannon's information theory, cross-entropy is mainly used to measure the difference in information between two probability distributions [66,67]. Let $P = \{p_1, p_2, \ldots, p_n\}$ and $Q = \{q_1, q_2, \ldots, q_n\}$ be two probability distributions defined over the same set of values. The cross-entropy between P and Q can be calculated as follows:

$$D(P,\ Q)=\sum_{i=1}^{N}p_i\log\frac{p_i}{q_i} \tag{16}$$

The minimum cross-entropy algorithm determines the threshold value by minimizing the cross-entropy between the original image and the thresholded image [68]. The lower the cross-entropy value, the lower the uncertainty and the greater the homogeneity. Let the original image be I, and $h(i)$, $i = 1, 2, \ldots, L$, is the corresponding histogram with L being

the number of grey levels. Then the thresholded image I_{th} is created by the threshold value th using the following equations:

$$I_{th} = \begin{cases} \mu(1,\ th), & if\ I(x,y) < th \\ \mu(th,\ L+1), & if\ I(x,y) \geq th \end{cases} \tag{17}$$

$$\mu(a,b) = \frac{\sum_{i=a}^{b-1} ih(i)}{\sum_{i=a}^{b-1} h(i)} \tag{18}$$

The thresholded image is generated based on Equation (17), then we can calculate the cross-entropy by rewriting Equation (17) as an objective function (also called fitness), which is listed below:

$$f_{cross}(th) = \sum_{i=1}^{th-1} ih(i) \log\left(\frac{i}{\mu(1,\ th)}\right) + \sum_{i=th}^{L} ih(i) \log\left(\frac{i}{\mu(th,\ L+1)}\right) \tag{19}$$

The above objective function considers a single threshold value to segment a given image, i.e., bi-level thresholding, it also can be extended to a multi-level approach for image segmentation, called multi-level thresholding image segmentation. Thus, the Equation (19) can be expressed as:

$$f_{cross}(th) = \sum_{i=1}^{L} ih(i) \log(i) - \sum_{i=1}^{nt} H_i \tag{20}$$

where $th = [th_1, th_2, \ldots, th_{nt}]$ indicates an array containing nt different threshold values. H_i is defined as follows:

$$H_1 = \sum_{i=1}^{th_1-1} ih(i) \log(\mu(1,\ th_1)) \tag{21}$$

$$H_k = \sum_{i=th_{k-1}}^{th_k-1} ih(i) \log(\mu(th_{k-1},\ th_k)),\ 1 < k < nt \tag{22}$$

$$H_{nt} = \sum_{i=th_{nt}}^{L} ih(i) \log(\mu(th_{nt},\ L+1)) \tag{23}$$

4. The Proposed Algorithm

4.1. The Details of MROA

Although ROA is easy to implement, suitable for solving optimization tasks widely, and provides more reliable results than other Mas, it has insufficient searchability (exploration and exploitation) in solving complex optimization problems; for example, it easily stagnates into optimal local solutions and has a slow convergence speed. Motivated by these considerations, this paper proposes a modified ROA algorithm called MROA for global optimization and multi-level thresholding image segmentation. There are two major strategies for modifying. First, Brownian motion is introduced to improve the exploration ability and provide a greater opportunity to find the optimal or near-optimal solution in the search space. Second, LOBL is used to improve the exploitation ability and accelerate the convergence rate of ROA. Therefore, the exploration phase of ROA is modified using Brownian motion, which is expressed as:

$$X(t+1) = \text{Brownian} \times X_{best}(t) - (rand \times (\frac{X_{best}(t) + X_{rand}(t)}{2}) - X_{rand}(t)) \tag{24}$$

where Brownian indicates Brownian motion.

The pseudo-code of MROA is presented in Algorithm 2, and Figure 4 illustrates the flowchart of MROA.

Algorithm 2 the pseudo-code of MROA

Inputs: N and T
Outputs: best solution
Initialize the positions of remora X_i (i = 1,2, . . . , N);
While ($t \leq T$)
  Check if any search agent goes beyond the search space and amend it;
  Apply LOBL strategy to generate lens-opposite solution by Equation (15);
  Evaluate candidate solution and select the best position by greedy strategy.
  For each remora indexed by i
    If H(i) == 0 **then**
      Using Equation (4) to update the position of attached whales;
    Elseif H(i) == 1 **then**
      Using Equation (24) to update the position of attached sailfishes;
    End if
    If $f(X_{att}) < f(X)$ **then**
      $X = X_{att}$;
      H(i) = round($rand$);
    Else
      Using Equation (8) to update the position of search agents;
    End if
  End for
End While

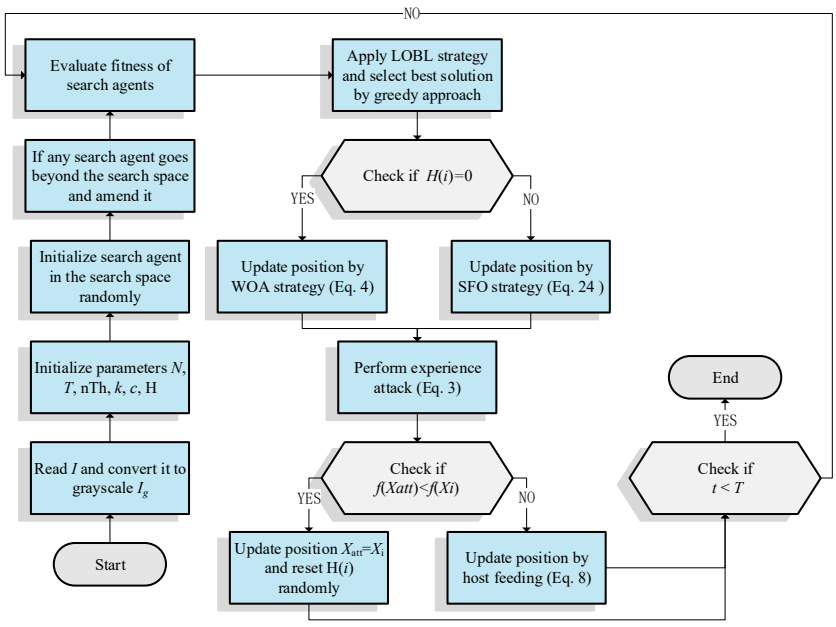

Figure 4. Flowchart of the proposed MROA.

4.2. The Proposed MROA for Solving Multi-Level Thresholding Image Segmentation Task

In this subsection, the MROA is employed to solve the multi-level thresholding image segmentation task and cross-entropy is used to determine optimal threshold values. We present the different steps of this method as below:

Step 1: Read image I and convert it to grayscale I_g, calculate the histogram h of I_g.
Step 2: Initialize the parameters of MROA: N, T, C, k, and random array H.
Step 3: Initialize the location of search agents with N population size and nTh dimensions.
Step 4: If any search agent goes beyond the search space and amend it.

Step 5: Evaluate the cross-entropy with Equation (20) for each search agent.

Step 6: Apply LOBL strategy to generate lens opposite solution and select the best one between the original and its opposite solution according to the fitness value.

Step 7: Select the appropriate host to update the location of the search agent according to the value of the H.

Step 8: The t index is increased in 1, if the stop criteria ($t \geq T$) are satisfied then output the best threshold values, otherwise jump to Step 5.

Step 9: Generate the segmented image *Seg* with the best threshold values obtained by MROA.

4.3. Computation Complexity of MROA

In the initialization phase, MROA produces the search agents randomly in the search space, so the computational complexity of this phase is O($N \times D$), where N denotes the number of population and D denotes the dimension size. Afterward, MROA evaluates each individual's fitness during the whole iteration with the complexity O($T \times N \times D$), where T indicates the number of iterations. Finally, for position updating, the complexity is summarized as O($T \times N \times D$). In summary, the total computational complexity of MROA is O($T \times N \times D$), which is the same as the original.

5. Experimental Results for Global Optimization

This section evaluates the optimization performance of the proposed MROA using 23 benchmark functions. First, the definitions of the 23 benchmark functions are introduced. Second, the experimental setup and comparison group including other well-known MAs are described in detail. Finally, the experimental results are analyzed and discussed.

5.1. Definition of 23 Benchmark Functions

To evaluate the searchability of the proposed MROA, 23 benchmark functions are introduced in this paper [15]. These functions are categorized into: (1) unimodal functions (F1–F7), (2) multimodal functions (F8–F14), and (3) fixed-dimension multimodal functions. These functions are defined in Table 1, where D, UM, and MM indicate the dimension, unimodal, and multimodal functions, respectively. Figure 5 shows the visualization of these functions. We can see that the unimodal functions have only one global optimal solution, which is available to evaluate the exploitation ability of MAs. By contrast, multimodal and fixed-dimension multimodal functions have many local optimal and only one global optimal solution, which is available to evaluate the exploration and ability to escape from the local optimal solution of MAs.

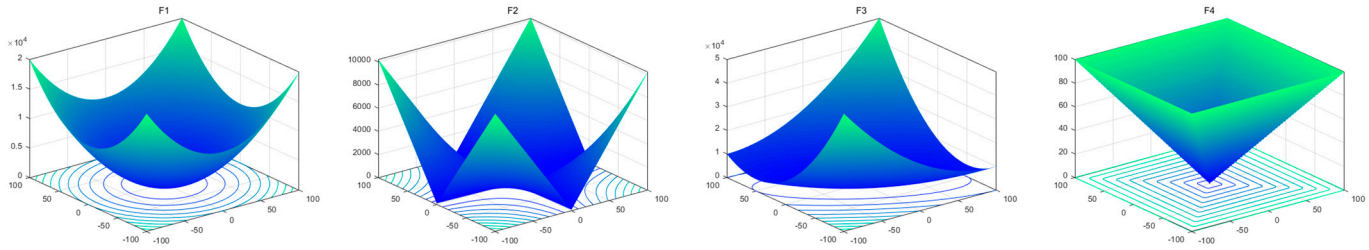

Figure 5. *Cont.*

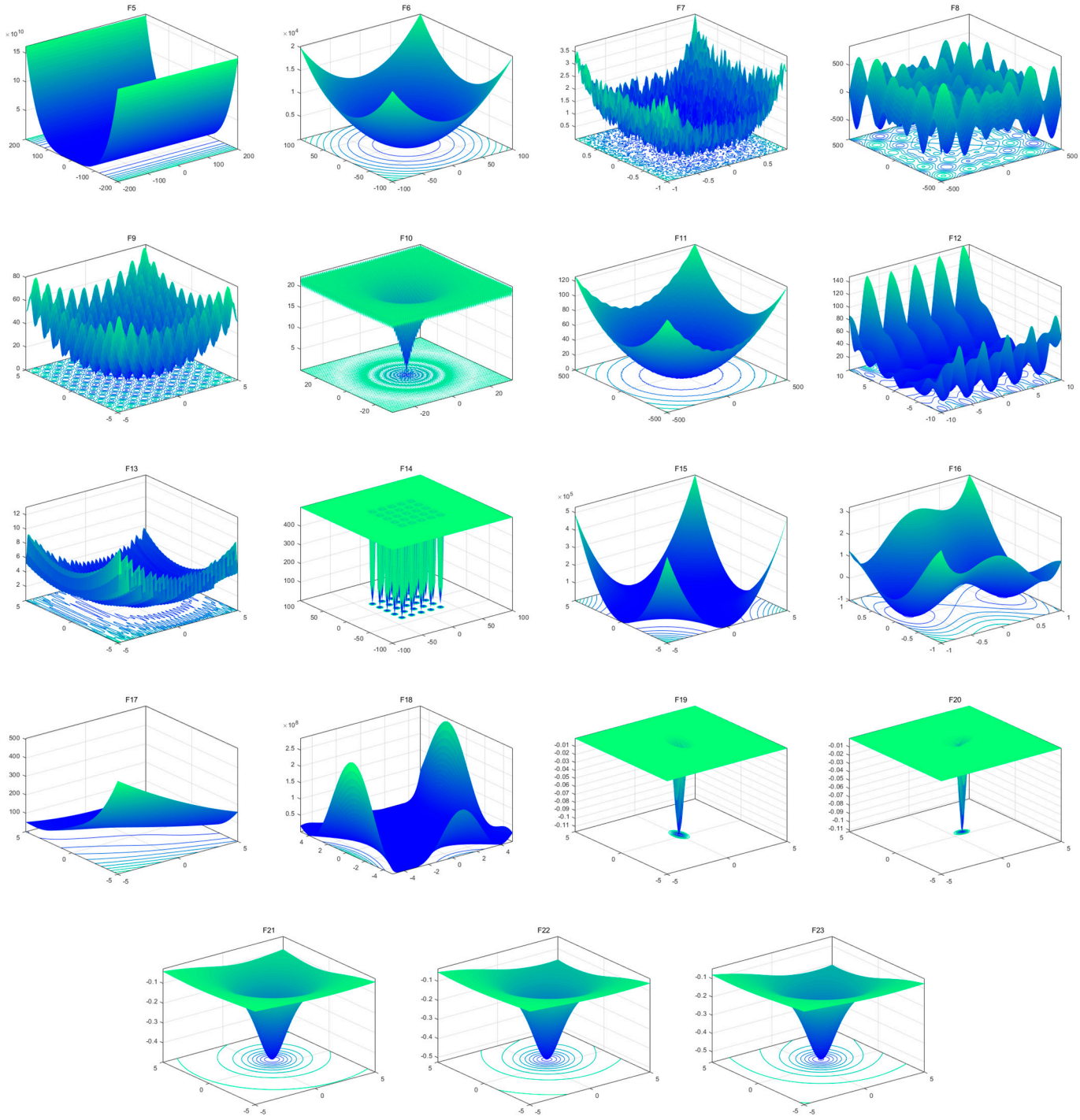

Figure 5. View of 23 benchmark functions.

Table 1. Definition of 23 benchmark functions.

No	Name	D	Range	Type	f_{min}
F1	Sphere	30	[−100, 100]	UM	0
F2	Schwefel 2.22	30	[−10, 10]	UM	0
F3	Schwefel 1.2	30	[−100, 100]	UM	0
F4	Schwefel 2.21	30	[−100, 100]	UM	0
F5	Rosenbrock	30	[−30, 30]	UM	0
F6	Step	30	[−100, 100]	UM	0
F7	Quartic	30	[−1.28, 1.28]	UM	0
F8	Schwefel	30	[−500, 500]	MM	−12,569.487
F9	Rastrigin	30	[−5.12, 5.12]	MM	0
F10	Ackley	30	[−32, 32]	MM	0
F11	Griewank	30	[−600, 600]	MM	0
F12	Penalized	30	[−50, 50]	MM	0
F13	Penalized 2	30	[−50, 50]	MM	0
F14	Foxholes	2	[−65.536, 65.536]	MM	0.998004
F15	Kowalik	4	[−5, −5]	MM	0.0003075
F16	Six-hump camel-back	2	[−5, −5]	MM	−1.0316285
F17	Branin	2	[−5, −5]	MM	0.398
F18	Goldstein-Price	2	[−2, 2]	MM	3
F19	Hartman 3	3	[−1, 2]	MM	−3.862782
F20	Hartman 6	6	[0, 1]	MM	−3.32236
F21	Shekel 5	4	[0, 10]	MM	−10.1532
F22	Shekel 7	4	[0, 10]	MM	−10.4029
F23	Shekel 10	4	[0, 10]	MM	−10.5364

5.2. Experimental Setup

As stated above, the 23 benchmark functions are utilized to evaluate the optimization performance of the proposed work. To show the representativeness of experimental results, the proposed algorithm MROA is compared with the original ROA [52] and other well-known MAs, including RSA [69], AOA [47], AO [35], SSA [31], SCA [45], and GWO [27]. For fair evaluation, we set the number of maximum iteration T = 500, population size N = 30, and dimension size D = 30, respectively. Moreover, all the tests are run 30 times independently. The best results are highlighted in bold. Table 2 represents the parameter setting of each algorithm and the details of these algorithms are listed as follows:

- ROA [52]: Simulates remora's parasitic behavior on hosts, such as whales and swordfish, to finish the predation behavior.
- RSA [69]: mimics the encircling and hunting mechanism of a crocodile swarm during foraging.
- AOA [47]: simulates the behavior of arithmetic operators in nature, which include multiplication (×), division (÷), addition (+), subtraction (−).
- AO [35]: inspired by the different hunting behavior of Aquila hawks in nature.
- SSA [31]: simulates the swarming behavior of salps during moving and foraging in the ocean.
- SCA [45]: simulates the common mathematical models, sine and cosine functions.
- GWO [27]: mimics the hunting strategy and leadership hierarchy of gray wolves.

Table 2. Parameter settings for each algorithm.

Algorithm	Parameters
MROA	$c = 0.1$; $k = 10{,}000$
ROA [52]	$c = 0.1$
RSA [69]	$\alpha = 0.1$; $\beta = 0.1$
AOA [47]	$\alpha = 5$; $\mu = 0.5$;
AO [35]	$U = 0.00565$; $c = 10$; $\omega = 0.005$; $\alpha = 0.1$; $\delta = 0.1$;
SSA [31]	$c_1 = [1, 0]$; $c_2 \in [0, 1]$; $c_3 \in [0, 1]$
SCA [45]	$A = 2$
GWO [27]	$a = [2, 0]$

5.3. Statistical Results on 23 Benchmark Functions

This subsection compared MROA with seven basic algorithms on 23 benchmark functions in terms of the mean value (Mean) and standard deviation (Std). The experimental results are given in Table 3. By observing this table, we can see that MROA has the smallest Mean and Std values among the most functions. Specifically, for F1–F4, MROA obtains the theoretical optimal solution, where ROA only finds the optimal solution, which shows the LOBL strategy effectively enhances the exploitation ability of MROA, and the lens opposite solution increases the diversity of the population, helping the search agents to jump out of the local optimal solution. For MM functions, MROA also provides more competitive results than seven well-known algorithms; the Brownian motion strategy improves the ROA's exploration capability and provides search agents with a greater opportunity to find the optimal or near-optimal solution in the search space. For F8, although MROA only finds the near-optimal solution, its convergence accuracy is also better than others. For F9, F10, and F11, MROA obtains the theoretically optimal solution. For F12, F13, and F4, the accuracy of MROA is weaker than AO and SSA, respectively. For F15–F23, MROA also provides a higher convergence accuracy than others. Moreover, Figure 6 shows the MROA and competitor algorithms' ranking in UM and MM functions. We can see from the results that the proposed MROA outperforms in most benchmark functions.

Furthermore, owing to the MAs being stochastic algorithms, in this paper, we consider the Wilcoxon rank-sum test to supplement our statistical analysis and evaluate the statistical significance of the results [70]. The Wilcoxon rank-sum test is a non-parametric test used to compare the results of each pair of algorithms. The test is based on two hypotheses: null and alternative. The null hypothesis indicates that there is no difference between the two samples. The alternative hypothesis indicates that there is a significant difference between the two samples. We set the significance level as 5%; according to this criterion, if the p-value is higher than 0.05, which indicates the null hypothesis is true, the significant difference is not obvious. If the p-value is less than 0.05, which indicates there is a significant difference, the null hypothesis is rejected. Furthermore, NaN denotes that there is no difference between the two samples. Table 4 shows the p-values obtained using the Wilcoxon rank-sum test, which is calculated by the fitness values between MROA and each of the algorithms included, presenting six different pairs, MROA vs. ROA, MROA vs. RSA, MROA vs. AOA, MROA vs. AO, MROA vs. SSA, MROA vs. SCA, and MROA vs. GWO. This table shows that the results of MROA are statistically significant for most benchmark functions, which indicates that the performance of MROA is not random. Consequently, based on the above analysis, we conclude that the MROA outperforms other algorithms for most benchmark functions in terms of convergence accuracy and statistical significance.

Table 3. Statistical results of algorithms on 23 benchmark functions.

Function		MROA	ROA	RSA	AOA	AO	SSA	SCA	GWO
F1	Mean	**0.00 × 10^{+00}**	8.88 × 10^{-314}	**0.00 × 10^{+00}**	5.22 × 10^{-06}	6.58 × 10^{-102}	2.03 × 10^{-07}	1.76 × 10^{+01}	1.23 × 10^{-27}
	Std	0.00 × 10^{+00}	0.00 × 10^{+00}	0.00 × 10^{+00}	2.58 × 10^{-06}	3.59 × 10^{-101}	2.30 × 10^{-07}	5.31 × 10^{+01}	2.21 × 10^{-27}
F2	Mean	**0.00 × 10^{+00}**	1.01 × 10^{-168}	**0.00 × 10^{+00}**	1.86 × 10^{-03}	1.72 × 10^{-59}	2.02 × 10^{+00}	2.95 × 10^{-02}	1.19 × 10^{-16}
	Std	0.00 × 10^{+00}	0.00 × 10^{+00}	0.00 × 10^{+00}	1.77 × 10^{-03}	9.40 × 10^{-59}	1.56 × 10^{+00}	5.07 × 10^{-02}	8.16 × 10^{-17}
F3	Mean	**0.00 × 10^{+00}**	1.15 × 10^{-268}	**0.00 × 10^{+00}**	1.10 × 10^{-03}	3.11 × 10^{-101}	1.67 × 10^{+03}	1.01 × 10^{+04}	1.60 × 10^{-04}
	Std	0.00 × 10^{+00}	0.00 × 10^{+00}	0.00 × 10^{+00}	8.16 × 10^{-04}	1.64 × 10^{-100}	8.80 × 10^{+02}	6.49 × 10^{+03}	8.16 × 10^{-04}
F4	Mean	**0.00 × 10^{+00}**	4.59 × 10^{-164}	**0.00 × 10^{+00}**	1.86 × 10^{-02}	2.13 × 10^{-53}	1.07 × 10^{+01}	3.79 × 10^{+01}	6.77 × 10^{-07}
	Std	0.00 × 10^{+00}	0.00 × 10^{+00}	0.00 × 10^{+00}	1.30 × 10^{-02}	9.90 × 10^{-53}	4.18 × 10^{+00}	1.10 × 10^{+01}	6.21 × 10^{-07}
F5	Mean	2.74 × 10^{+01}	2.63 × 10^{+01}	2.13 × 10^{+01}	2.81 × 10^{+01}	**7.19 × 10^{-03}**	3.22 × 10^{+02}	6.92 × 10^{+04}	2.70 × 10^{+01}
	Std	6.30 × 10^{-01}	4.96 × 10^{+00}	1.30 × 10^{+01}	2.22 × 10^{-01}	1.18 × 10^{-02}	6.84 × 10^{+02}	1.81 × 10^{+05}	6.69 × 10^{-01}
F6	Mean	5.72 × 10^{-01}	1.05 × 10^{-01}	7.35 × 10^{+00}	3.10 × 10^{+00}	1.23 × 10^{-04}	**2.33 × 10^{-07}**	1.96 × 10^{+01}	7.63 × 10^{-01}
	Std	2.48 × 10^{-01}	7.73 × 10^{-02}	2.90 × 10^{-01}	2.37 × 10^{-01}	1.84 × 10^{-04}	3.20 × 10^{-07}	2.77 × 10^{+01}	3.27 × 10^{-01}
F7	Mean	**5.95 × 10^{-05}**	1.64 × 10^{-04}	1.02 × 10^{-04}	7.00 × 10^{-05}	1.12 × 10^{-04}	1.68 × 10^{-01}	9.58 × 10^{-02}	1.80 × 10^{-03}
	Std	6.00 × 10^{-05}	1.88 × 10^{-04}	1.16 × 10^{-04}	7.00 × 10^{-05}	8.14 × 10^{-05}	6.99 × 10^{-02}	8.56 × 10^{-02}	9.21 × 10^{-04}
F8	Mean	**−1.24 × 10^{+04}**	−1.23 × 10^{+04}	−5.34 × 10^{+03}	−5.50 × 10^{+03}	−8.43 × 10^{+03}	−7.10 × 10^{+03}	−3.80 × 10^{+03}	−6.09 × 10^{+03}
	Std	2.60 × 10^{+02}	4.96 × 10^{+02}	3.88 × 10^{+02}	4.21 × 10^{+02}	3.55 × 10^{+03}	8.77 × 10^{+02}	2.56 × 10^{+02}	8.92 × 10^{+02}
F9	Mean	**0.00 × 10^{+00}**	**0.00 × 10^{+00}**	**0.00 × 10^{+00}**	1.60 × 10^{-06}	**0.00 × 10^{+00}**	5.90 × 10^{+01}	2.98 × 10^{+01}	3.34 × 10^{+00}
	Std	0.00 × 10^{+00}	0.00 × 10^{+00}	0.00 × 10^{+00}	1.51 × 10^{-06}	0.00 × 10^{+00}	2.59 × 10^{+01}	2.55 × 10^{+01}	4.09 × 10^{+00}
F10	Mean	**8.88 × 10^{-16}**	**8.88 × 10^{-16}**	**8.88 × 10^{-16}**	4.71 × 10^{-04}	**8.88 × 10^{-16}**	2.49 × 10^{+00}	1.42 × 10^{+01}	1.07 × 10^{-13}
	Std	0.00 × 10^{+00}	0.00 × 10^{+00}	0.00 × 10^{+00}	1.40 × 10^{-04}	0.00 × 10^{+00}	9.35 × 10^{-01}	8.86 × 10^{+00}	1.60 × 10^{-14}
F11	Mean	**0.00 × 10^{+00}**	**0.00 × 10^{+00}**	**0.00 × 10^{+00}**	3.13 × 10^{-03}	**0.00 × 10^{+00}**	1.97 × 10^{-02}	1.17 × 10^{+00}	5.43 × 10^{-03}
	Std	0.00 × 10^{+00}	0.00 × 10^{+00}	0.00 × 10^{+00}	1.19 × 10^{-02}	0.00 × 10^{+00}	1.53 × 10^{-02}	7.83 × 10^{-01}	8.53 × 10^{-03}
F12	Mean	4.41 × 10^{-02}	1.11 × 10^{-02}	1.55 × 10^{+00}	7.46 × 10^{-01}	**2.73 × 10^{-06}**	6.64 × 10^{+00}	4.05 × 10^{+04}	3.83 × 10^{-02}
	Std	2.34 × 10^{-02}	1.09 × 10^{-02}	3.31 × 10^{-01}	3.10 × 10^{-02}	3.94 × 10^{-06}	3.35 × 10^{+00}	1.54 × 10^{+05}	1.52 × 10^{-02}
F13	Mean	2.44 × 10^{+00}	2.13 × 10^{-01}	3.85 × 10^{-01}	2.96 × 10^{+00}	**6.09 × 10^{-05}**	1.81 × 10^{+01}	3.82 × 10^{+05}	6.87 × 10^{-01}
	Std	1.07 × 10^{+00}	1.29 × 10^{-01}	9.99 × 10^{-01}	1.99 × 10^{-02}	1.03 × 10^{-04}	1.52 × 10^{+01}	1.23 × 10^{+06}	1.90 × 10^{-01}
F14	Mean	9.57 × 10^{+00}	3.22 × 10^{+00}	4.54 × 10^{+00}	1.07 × 10^{+01}	2.82 × 10^{+00}	**1.10 × 10^{+00}**	1.66 × 10^{+00}	5.50 × 10^{+00}
	Std	4.85 × 10^{+00}	3.89 × 10^{+00}	3.51 × 10^{+00}	3.15 × 10^{+00}	3.97 × 10^{+00}	3.03 × 10^{-01}	9.48 × 10^{-01}	4.28 × 10^{+00}
F15	Mean	**4.32 × 10^{-04}**	4.33 × 10^{-04}	2.85 × 10^{-03}	1.29 × 10^{-02}	4.57 × 10^{-04}	2.81 × 10^{-03}	1.22 × 10^{-03}	3.75 × 10^{-03}
	Std	1.59 × 10^{-04}	1.96 × 10^{-04}	1.63 × 10^{-03}	2.88 × 10^{-02}	9.57 × 10^{-05}	5.96 × 10^{-03}	3.42 × 10^{-04}	7.56 × 10^{-03}
F16	Mean	**−1.03 × 10^{+00}**	**−1.03 × 10^{+00}**	**−1.03 × 10^{+00}**	**−1.03 × 10^{+00}**	−1.03 × 10^{+00}	**−1.03 × 10^{+00}**	**−1.03 × 10^{+00}**	**−1.03 × 10^{+00}**
	Std	2.30 × 10^{-08}	3.47 × 10^{-08}	1.97 × 10^{-03}	2.22 × 10^{-11}	3.91 × 10^{-04}	1.81 × 10^{-14}	4.59 × 10^{-05}	2.85 × 10^{-08}
F17	Mean	**3.98 × 10^{-01}**	**3.98 × 10^{-01}**	4.17 × 10^{-01}	4.03 × 10^{-01}	3.98 × 10^{-01}	**3.98 × 10^{-01}**	3.99 × 10^{-01}	**3.98 × 10^{-01}**
	Std	7.33 × 10^{-06}	5.30 × 10^{-06}	1.59 × 10^{-02}	2.50 × 10^{-02}	1.88 × 10^{-04}	1.12 × 10^{-14}	1.15 × 10^{-03}	9.65 × 10^{-07}
F18	Mean	**3.00 × 10^{+00}**	**3.00 × 10^{+00}**	6.68 × 10^{+00}	3.06 × 10^{+01}	3.04 × 10^{+00}	**3.00 × 10^{+00}**	**3.00 × 10^{+00}**	**3.00 × 10^{+00}**
	Std	1.23 × 10^{-04}	7.58 × 10^{-05}	9.55 × 10^{+00}	3.49 × 10^{+01}	4.04 × 10^{-02}	2.32 × 10^{-13}	1.92 × 10^{-04}	3.62 × 10^{-05}
F19	Mean	**−3.86 × 10^{+00}**	−3.86 × 10^{+00}	−3.76 × 10^{+00}	−3.77 × 10^{+00}	−3.86 × 10^{+00}	**−3.86 × 10^{+00}**	−3.85 × 10^{+00}	−3.86 × 10^{+00}
	Std	1.27 × 10^{-04}	2.73 × 10^{-03}	1.65 × 10^{-01}	5.23 × 10^{-01}	7.21 × 10^{-03}	2.50 × 10^{-12}	8.81 × 10^{-03}	3.81 × 10^{-03}
F20	Mean	**−3.30 × 10^{+00}**	−3.24 × 10^{+00}	−2.71 × 10^{+00}	−3.27 × 10^{+00}	−3.16 × 10^{+00}	−3.23 × 10^{+00}	−2.89 × 10^{+00}	−3.27 × 10^{+00}
	Std	4.51 × 10^{-02}	8.27 × 10^{-02}	2.93 × 10^{-01}	5.93 × 10^{-02}	1.09 × 10^{-01}	5.83 × 10^{-02}	3.16 × 10^{-01}	7.81 × 10^{-02}
F21	Mean	**−1.02 × 10^{+01}**	−1.01 × 10^{+01}	−5.06 × 10^{+00}	−7.71 × 10^{+00}	−1.01 × 10^{+01}	−7.23 × 10^{+00}	−2.53 × 10^{+00}	−8.98 × 10^{+00}
	Std	3.00 × 10^{-03}	1.45 × 10^{-02}	3.61 × 10^{-07}	2.69 × 10^{+00}	1.02 × 10^{-02}	3.48 × 10^{+00}	1.81 × 10^{+00}	2.44 × 10^{+00}
F22	Mean	**−1.04 × 10^{+01}**	−1.04 × 10^{+01}	−5.09 × 10^{+00}	−8.26 × 10^{+00}	−1.04 × 10^{+01}	−8.76 × 10^{+00}	−3.26 × 10^{+00}	−1.04 × 10^{+01}
	Std	2.02 × 10^{-03}	2.45 × 10^{-02}	7.16 × 10^{-07}	2.92 × 10^{+00}	1.45 × 10^{-02}	3.05 × 10^{+00}	1.85 × 10^{+00}	2.40 × 10^{-03}
F23	Mean	**−1.05 × 10^{+01}**	−1.05 × 10^{+01}	−5.13 × 10^{+00}	−7.35 × 10^{+00}	−1.05 × 10^{+01}	−8.85 × 10^{+00}	−3.65 × 10^{+00}	−1.01 × 10^{+01}
	Std	2.19 × 10^{-03}	1.97 × 10^{-02}	1.44 × 10^{-06}	3.38 × 10^{+00}	2.93 × 10^{-02}	2.90 × 10^{+00}	1.86 × 10^{+00}	1.85 × 10^{+00}

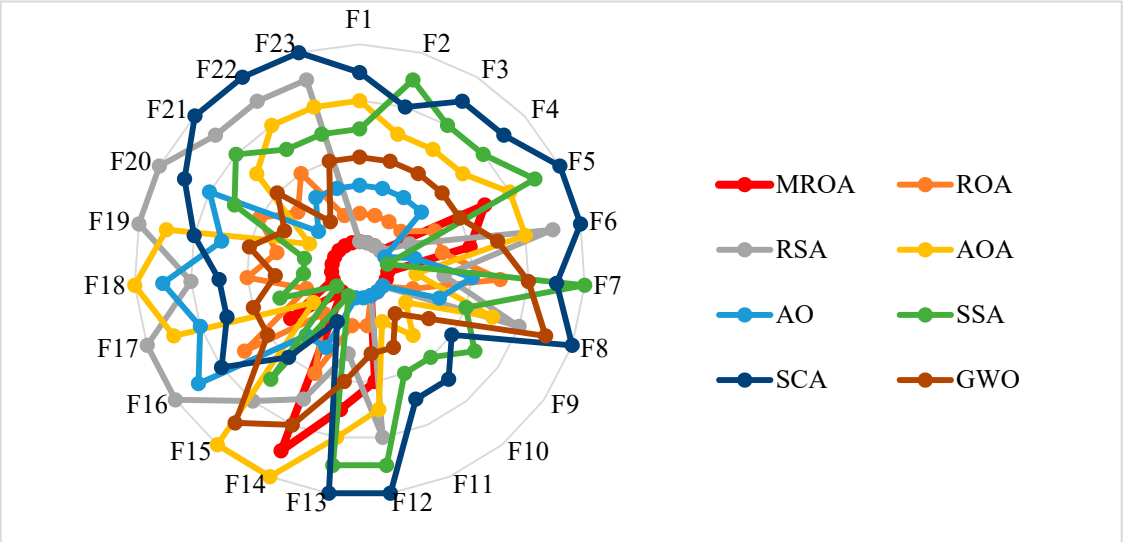

Figure 6. The radar graphs of algorithms on 23 benchmark functions.

Table 4. Statistical results of algorithms on 23 benchmark functions using Wilcoxon rank-sum test.

Function	MROA vs.						
	ROA	**RSA**	**AOA**	**AO**	**SSA**	**SCA**	**GWO**
F1	4.19×10^{-02}	NaN	1.21×10^{-12}	1.21×10^{-12}	1.21×10^{-12}	1.21×10^{-12}	1.21×10^{-12}
F2	1.21×10^{-12}	NaN	1.21×10^{-12}	1.21×10^{-12}	1.21×10^{-12}	1.21×10^{-12}	1.21×10^{-12}
F3	1.21×10^{-12}	NaN	1.21×10^{-12}	1.21×10^{-12}	1.21×10^{-12}	1.21×10^{-12}	1.21×10^{-12}
F4	1.21×10^{-12}	NaN	1.21×10^{-12}	1.21×10^{-12}	1.21×10^{-12}	1.21×10^{-12}	1.21×10^{-12}
F5	2.46×10^{-01}	2.50×10^{-02}	1.70×10^{-08}	3.02×10^{-11}	5.57×10^{-10}	3.02×10^{-11}	3.18×10^{-01}
F6	3.20×10^{-09}	1.79×10^{-11}	4.08×10^{-11}	3.02×10^{-11}	3.02×10^{-11}	3.02×10^{-11}	8.77×10^{-02}
F7	2.13×10^{-05}	3.92×10^{-02}	6.41×10^{-01}	8.50×10^{-02}	3.02×10^{-11}	3.02×10^{-11}	3.02×10^{-11}
F8	9.06×10^{-08}	3.01×10^{-11}	3.02×10^{-11}	9.33×10^{-02}	8.99×10^{-11}	3.02×10^{-11}	3.02×10^{-11}
F9	NaN	NaN	1.21×10^{-12}	NaN	1.21×10^{-12}	1.21×10^{-12}	1.18×10^{-12}
F10	NaN	NaN	1.21×10^{-12}	NaN	1.21×10^{-12}	1.21×10^{-12}	1.02×10^{-12}
F11	NaN	NaN	1.21×10^{-12}	NaN	1.21×10^{-12}	1.21×10^{-12}	1.10×10^{-02}
F12	3.16×10^{-10}	1.10×10^{-11}	3.02×10^{-11}	3.02×10^{-11}	3.02×10^{-11}	3.02×10^{-11}	1.30×10^{-03}
F13	3.16×10^{-10}	6.71×10^{-05}	9.51×10^{-06}	3.02×10^{-11}	2.75×10^{-03}	3.02×10^{-11}	1.03×10^{-06}
F14	3.37×10^{-06}	3.34×10^{-04}	3.91×10^{-01}	8.07×10^{-07}	2.18×10^{-10}	3.20×10^{-07}	4.56×10^{-05}
F15	3.18×10^{-01}	5.49×10^{-11}	1.22×10^{-01}	6.36×10^{-05}	6.70×10^{-11}	1.86×10^{-09}	5.69×10^{-01}
F16	1.77×10^{-03}	5.57×10^{-10}	3.02×10^{-11}	5.57×10^{-10}	3.01×10^{-11}	5.57×10^{-10}	1.08×10^{-02}
F17	3.71×10^{-01}	6.07×10^{-11}	3.02×10^{-11}	1.17×10^{-09}	2.86×10^{-11}	3.34×10^{-11}	2.90×10^{-01}
F18	5.08×10^{-03}	1.09×10^{-01}	3.99×10^{-04}	3.02×10^{-11}	3.02×10^{-11}	7.98×10^{-02}	7.24×10^{-02}
F19	9.06×10^{-08}	3.02×10^{-11}	1.86×10^{-03}	6.07×10^{-11}	3.02×10^{-11}	3.02×10^{-11}	2.25×10^{-04}
F20	4.01×10^{-02}	3.69×10^{-11}	6.77×10^{-05}	3.50×10^{-03}	3.26×10^{-01}	3.47×10^{-10}	2.05×10^{-03}
F21	3.01×10^{-07}	3.02×10^{-11}	3.37×10^{-04}	7.30×10^{-04}	1.86×10^{-01}	3.02×10^{-11}	5.26×10^{-04}
F22	1.17×10^{-09}	3.02×10^{-11}	9.53×10^{-07}	1.47×10^{-07}	3.99×10^{-04}	3.02×10^{-11}	6.05×10^{-07}
F23	8.48×10^{-09}	3.02×10^{-11}	1.27×10^{-02}	5.19×10^{-07}	9.51×10^{-06}	3.02×10^{-11}	1.75×10^{-05}

5.4. Boxplot Behavior Analysis

To further validate the excellent performance of the proposed MROA, Figure 7 presents the boxplot behavior of MROA and other MAs for some functions, including UM and MM types. Since boxplots indicate the data distribution, it is available to describe the consistency between data. MROA is very narrow compared with other algorithms and maintains the lowest values for most functions. It is observed that ROA outperforms the other algorithms in terms of data distribution, but only on F6, F8, and F15; the performance is mediocre for data distribution.

5.5. Convergence Behavior Analysis

This subsection analyzed the convergence behavior of the proposed MROA with compared algorithms. The convergence curve of these algorithms on 23 benchmark functions is shown in Figure 8. From this figure, we can conclude that MROA outperforms other well-known MAs in terms of convergence speed and optimization accuracy. For unimodal functions F1, F2, and F4, MROA achieves the fastest convergence speed and obtains the theoretically optimal solutions. However, for F6, the performance of MROA is not excellent and it may be trapped into the local optimal. For F7, although MROA cannot obtain the theoretical optimal solution, it also finds the most near-optimal solution and shows the fastest convergence speed than others. For MM functions, MROA also shows excellent optimization performance than other popular methods. For F8, MROA has a significant convergence capability that exceeds two ROA and SSA methods. For F9 and F11, MROA finds the theoretical optimal solution and has a faster convergence speed than others. We concluded that MROA has an excellent convergence ability in UM and MM functions.

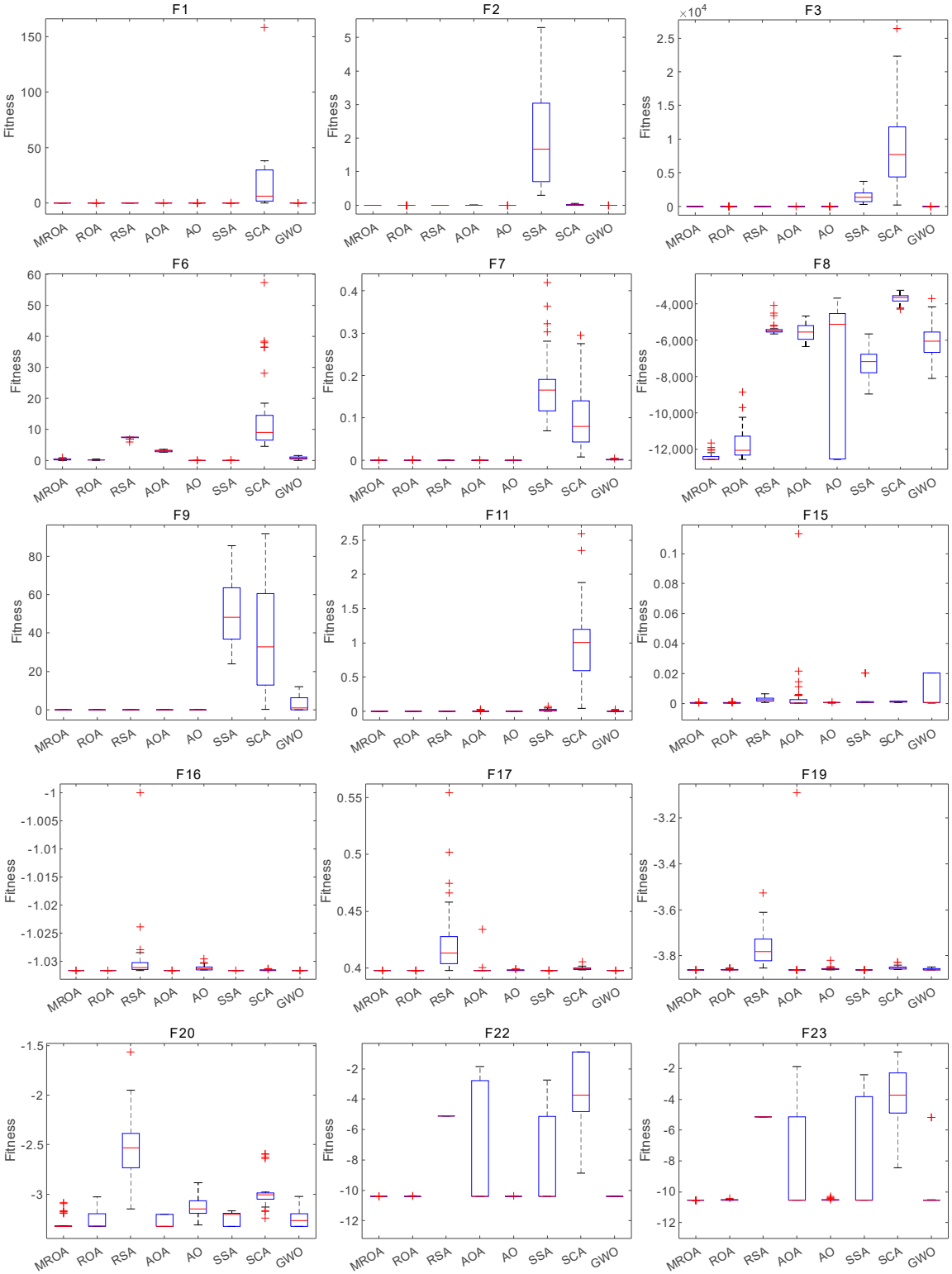

Figure 7. Boxplot behavior of algorithms on some functions.

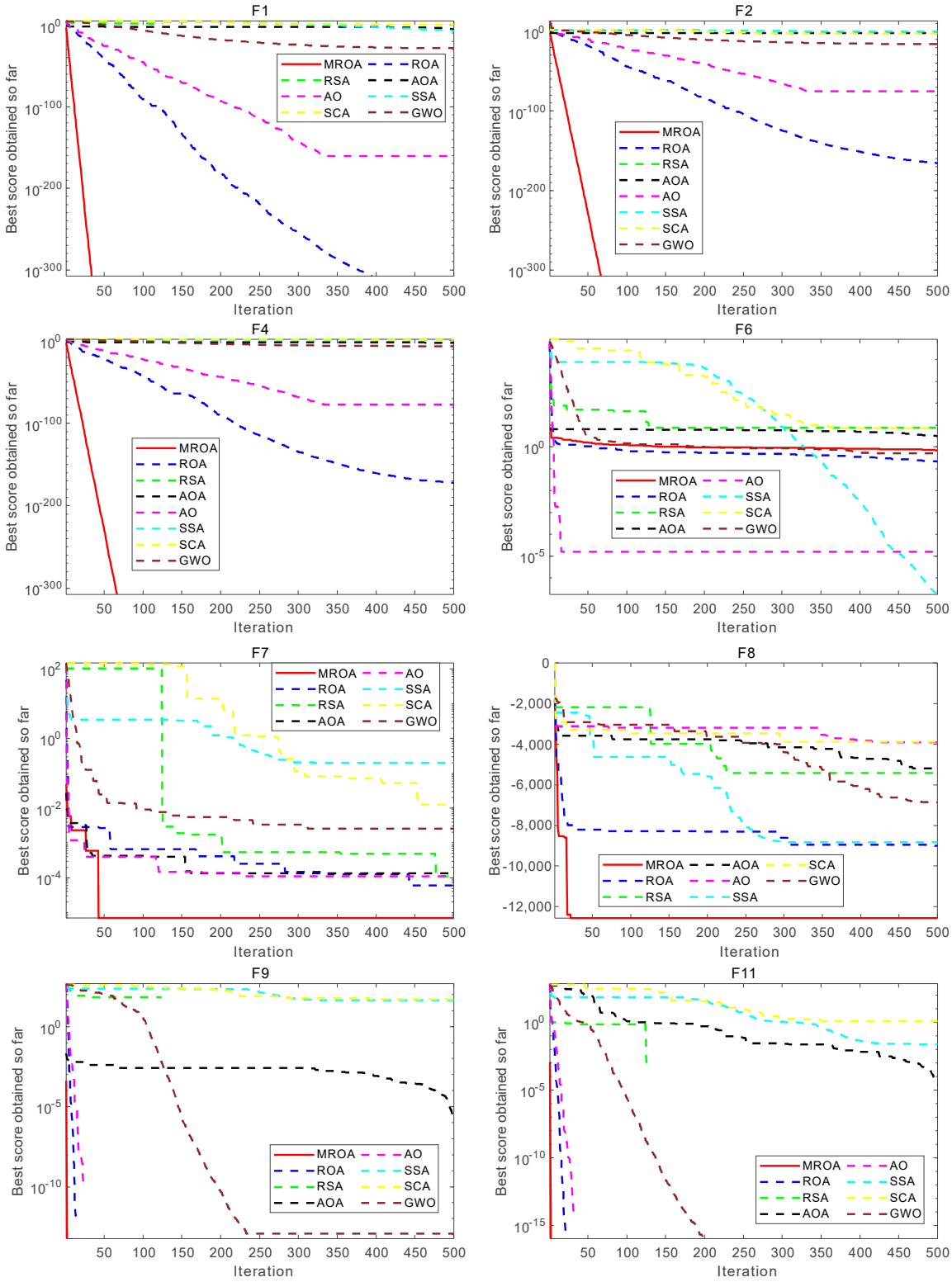

Figure 8. *Cont.*

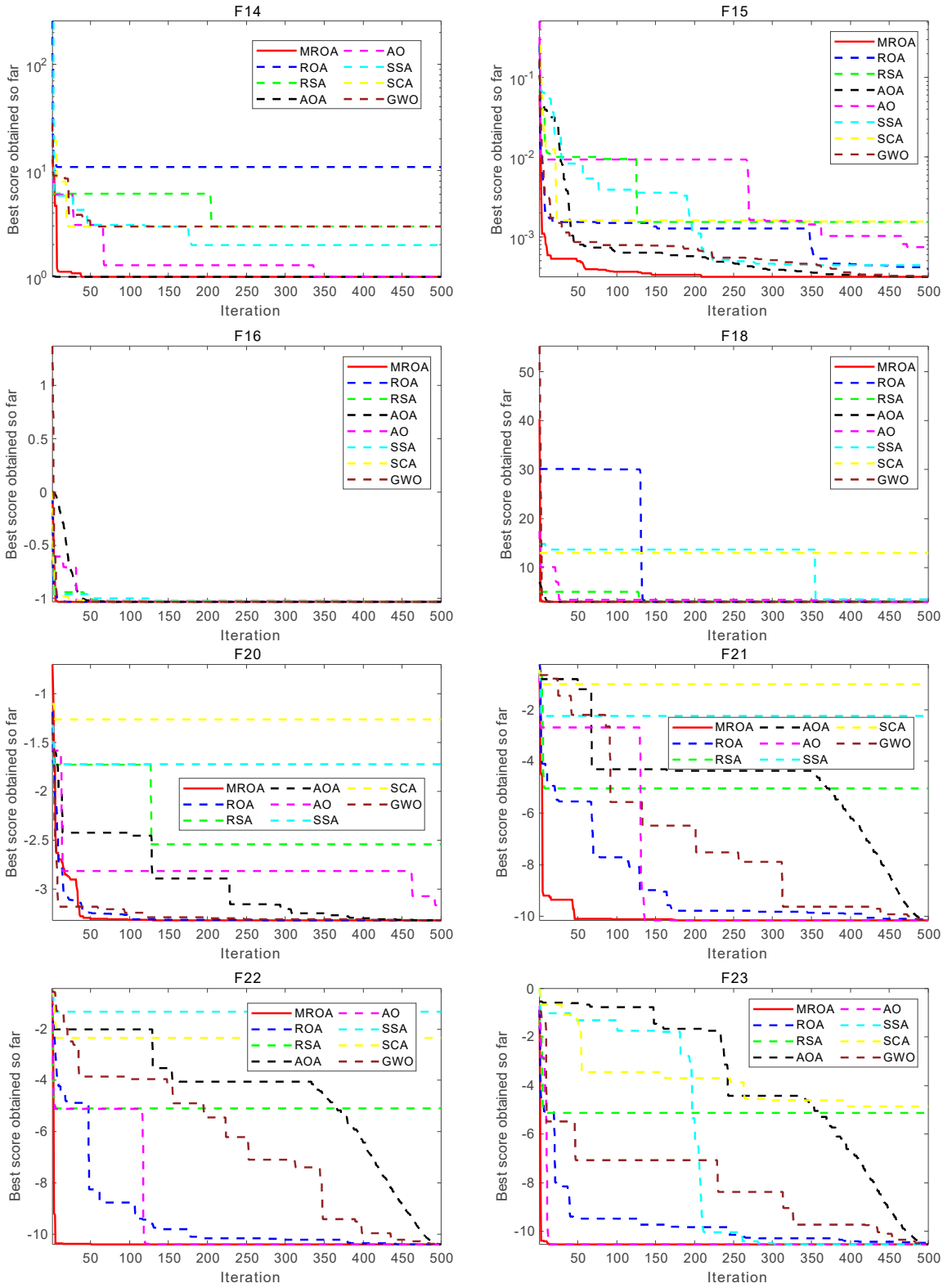

Figure 8. Convergence behavior of algorithms on some functions.

6. Experimental Results for Multi-Level Thresholding Image Segmentation

This section used MROA to minimize the cross-entropy for solving multi-level thresholding image segmentation tasks. First, we selected eight images from the Berkeley segmentation dataset [71] as the benchmark images and the experimental setup described in detail. Second, three image measurements, including *PSNR*, *SSIM*, and *FSIM* are introduced to measure the segmentation performance (quality, consistency, and accuracy) of MROA and other algorithms. Finally, the experimental results are discussed and analyzed.

6.1. Berkeley Segmentation Dataset

The proposed MROA with other algorithms is evaluated on eight images from the Berkeley segmentation dataset [71]. In this work, eight benchmark images are grayscale. These images and their histogram are presented in Figure 9. The purpose of selecting these images is only to test the algorithms' segmentation performance and quality.

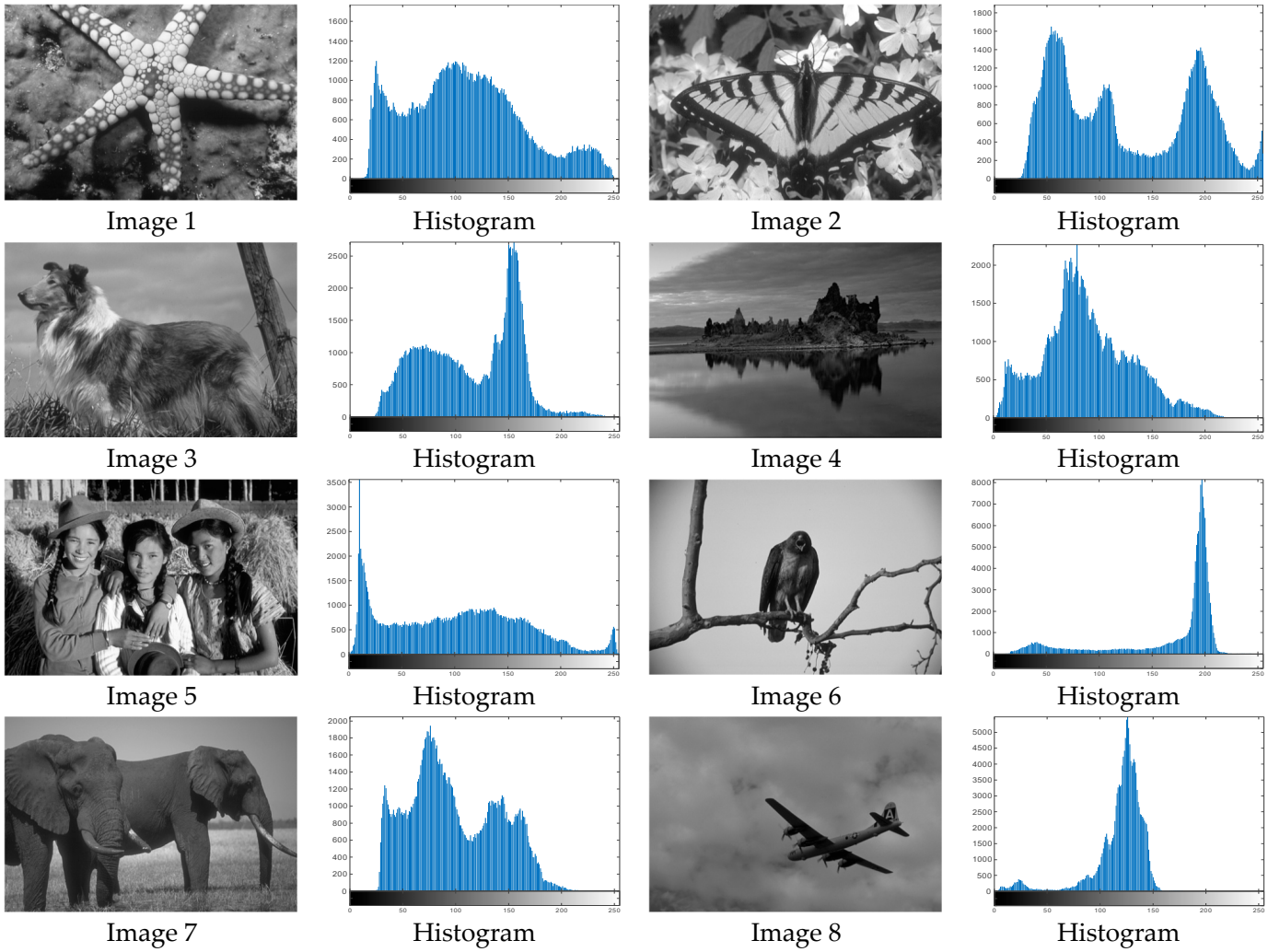

Figure 9. Berkeley image dataset and its histogram.

6.2. Experimental Setup

The proposed MROA is compared with seven well-known algorithms such as ROA [52], RSA [69], AOA [47], AO [35], SSA [31], SCA [45], and GWO [27]. The described parameters and settings of these algorithms are described in Section 4.2. For fair evaluation, the number of maximum iteration T = 500, the population size N = 30, and all the algorithms were run 30 times independently. The best values are highlighted in bold. All the images are segmented using different threshold values nTh = [4, 8, 12, 16].

6.3. Segmentation Quality Evaluation Measurements

6.3.1. Peak Signal-to-Noise Ratio (*PSNR*)

PSNR is used to calculate the ratio between the maximum possible signal power and the distorted noise power that affects the quality of its representation. The signal is regarded as the original data, and the noise is the error caused by segmentation. The *PSNR* is the most commonly used quality assessment technique to compare an original image and its segmented images using root mean square error (*RMSE*) per pixel. A higher *PSNR* indicates more similarity between the images, which is reflected in a better segmentation process [71,72]. It can be described as follows:

$$PSNR = 20log_{10}\frac{255}{RMSE} \tag{25}$$

$$RMSE = \sqrt{\frac{\sum_{i=1}^{M}\sum_{j=1}^{N}\left((I_g(i,j) - Seg(i,j)\right)^2)}{M \times N}} \tag{26}$$

where I_g and Seg denote the original and segmented image, respectively. M and N are the sizes of the image.

6.3.2. Structural Similarity (*SSIM*)

The *SSIM* is used to measure the degree of distortion of the images, and it can also measure the similarity from three perspectives, including luminance, contrast, and structural content between original and segmented images. Unlike mean-square error (*MSE*) and *PSNR*, *SSIM* measures absolute error, which is more in line with the intuitive feeling of the human eye [72,73]. *SSIM* is computed by the following equation:

$$SSIM(I_g, Seg) = \frac{(2\mu_{I_g}\mu_{Seg} + c_1)(2\sigma_{I_g,Seg} + c_2)}{({\mu_{I_g}}^2 + {\mu_{Seg}}^2 + c_1)({\sigma_{I_g}}^2 + {\sigma_{Seg}}^2 + c_2)} \tag{27}$$

where μ_I and μ_{Seg} indicate the mean intensities of the original and its segmented image, respectively. σ_I and σ_{Seg} are standard deviations of original and its segmented images. $\sigma_{I,\,Seg}$ is the covariance between original and segmented images. c_1 and c_2 are two constants equal to 0.065.

6.3.3. Feature Similarity (*FSIM*)

FSIM is a variant of *SSIM* that considers low-level features such as the gradient magnitude and phase congruency to measure the similarity of two images [74,75]. It can be described as follows:

$$FSIM = \frac{\sum_{\omega\in\Omega} S_L(\omega)PC_m(\omega)}{\sum_{\omega\in\Omega} PC_m(\omega)} \tag{28}$$

$$S_L(\omega) = S_{PC}(\omega)S_G(\omega) \tag{29}$$

$$S_{PC}(\omega) = \frac{2PC_1(\omega)PC_2(\omega) + T_1}{{PC_1}^2(\omega) + {PC_2}^2(\omega) + T_1} \tag{30}$$

$$S_G(\omega) = \frac{2G_1(\omega)G_2(\omega) + T_2}{{G_1}^2(\omega) + {G_2}^2(\omega) + T_2} \tag{31}$$

where Ω indicates the entire domain of the image. T_1 and T_2 are constants which equal to 0.85 and 160, respectively. *G* indicates the gradient magnitude of an image, and *PC* denotes the phase congruence.

6.4. Experimental Results Analysis of Benchmark Images

We compared MROA with other well-known algorithms for solving multi-level thresholding image segmentation tasks in this subsection. Cross-entropy is used as the objective function. Table A1 (in Appendix A) denotes the best threshold values obtained by algorithms at different threshold values. Table A2 contains the segmented images obtained from the proposed MROA at nTh = [4, 8, 12, 16]. Tables A3–A6 show the mean and standard deviation values for fitness, *PSNR*, *SSIM*, and *FSIM* obtained by algorithms, respectively. The higher mean values obtained indicate more optimization accuracy and efficiency of an algorithm.

On the other hand, the smaller the standard deviation values, the more stable the algorithm. Table A7 shows the Wilcoxon rank-sum results for fitness, the significance level is the same as Section 4.3. Moreover, Figures 10–13 show the summary average results obtained by algorithms in terms of fitness, *PSNR*, *SSIM*, and *FSIM*, respectively. Figure 14 summarized the best cases in terms of fitness, *PSNR*, *SSIM*, and *FSIM*, respectively.

It can be seen from Table A1 that in most cases, when the threshold level is 4 and 8, similar values are obtained by algorithms, especially for ROA, AO, SSA, and GWO. When the threshold level is 12 and 16, the difference is significant. According to Figure 10 and Table A3, the proposed work outperforms others in terms of average fitness and summarized. We conduct that MROA achieves the smallest fitness value in most cases at threshold values 8, 12, and 16.

Figure 10. Average fitness values obtained by the algorithms over all images.

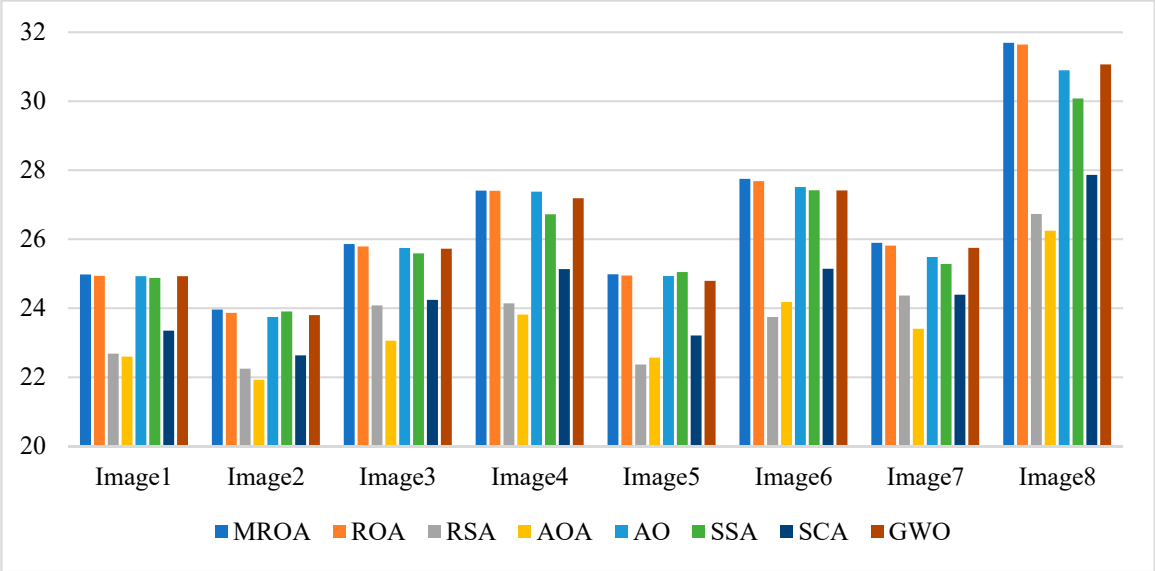

Figure 11. Average *PSNR* values obtained by the algorithms over all images.

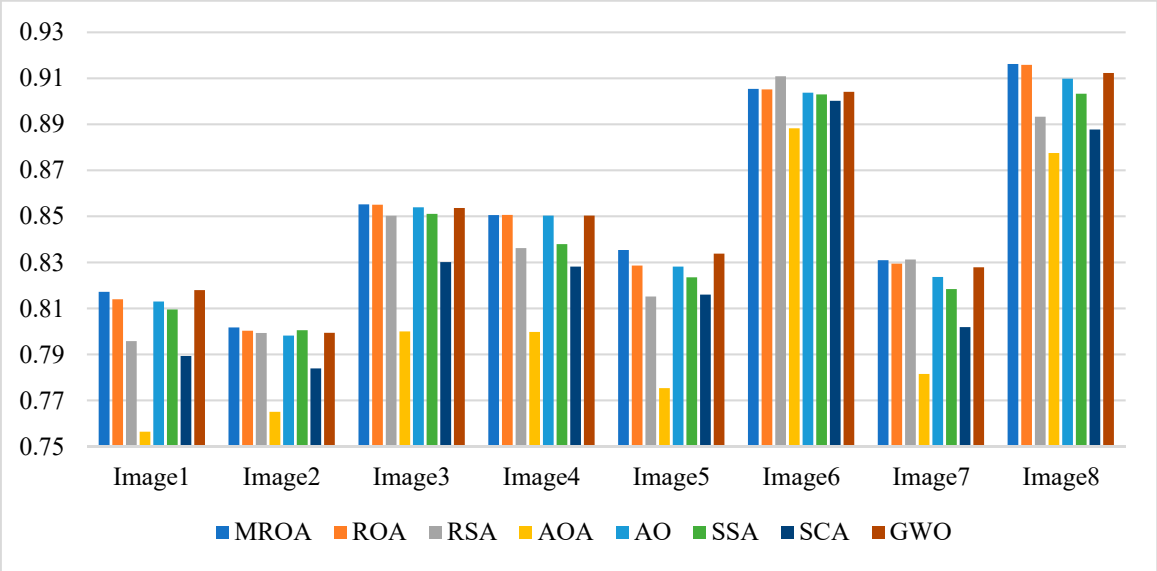

Figure 12. Average SSIM values obtained by the algorithms over all images.

Table A4 and Figure 11 show the mean *PSNR* values and a summary obtained by algorithms with different threshold values, respectively. It is available for evaluating the quality between the segmented image and the original. From this figure and table, we can see that the MROA has a significant advantage against ROA, AO, SSA, and GWO in most cases. The RSA, AOA, and SCA do not show excellent *PSNR* values. In the case of ROA, compared with other algorithms, as shown in Table A4, the *PSNR* values obtained for image 1, image 6, and image 8 present higher results at all levels. While segmenting image 2, image 3, image 4, and image 7, MROA outperforms others at three different levels.

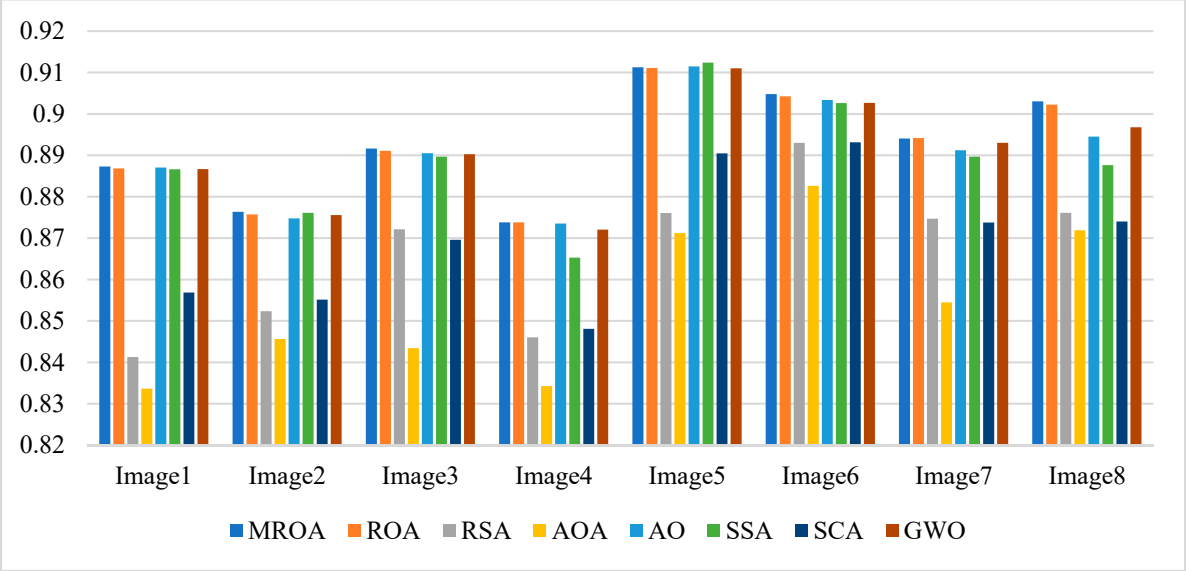

Figure 13. Average FSIM values obtained by the algorithms over all images.

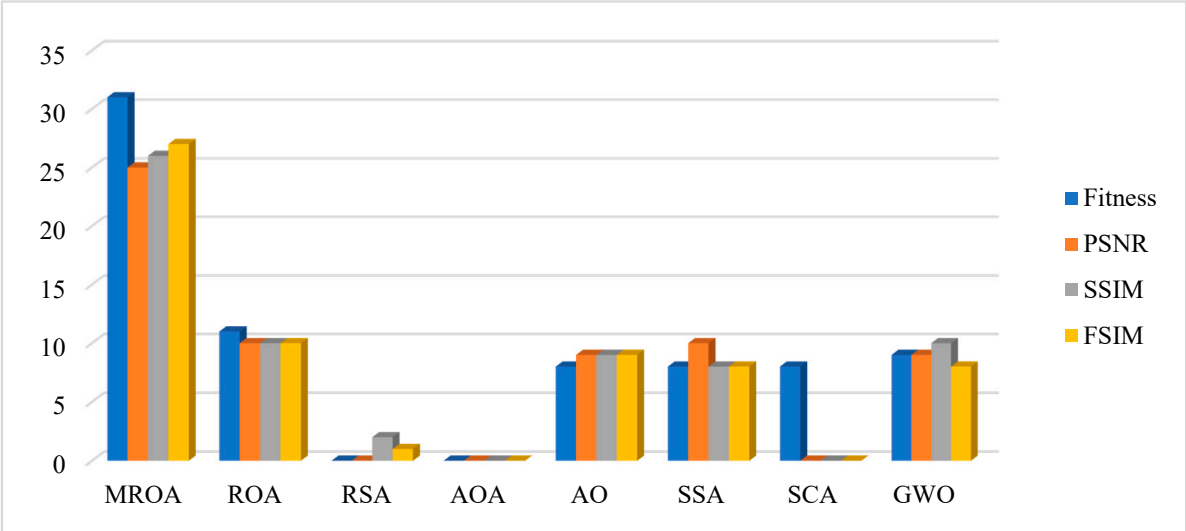

Figure 14. The number of best cases based on the fitness, *PSNR*, *SSIM*, *FSIM* obtained by algorithms over all images.

Table A5 and Figure 12 indicate the mean SSIM values and a summary obtained by algorithms at different threshold values, respectively. SSIM measures the similarity between two images. It can be seen that MROA outperforms others in terms of *PSNR* values. Specifically, for image 4, image 5, and image 8, MROA produces higher results at all levels. For image 1, image 2, image 6, and image 7, MROA outperforms others at three levels.

Table A6 and Figure 13 present the mean FSIM values and a summary obtained by algorithms at different threshold values, respectively. FSIM is a variant of SSIM used to evaluate the feature similarity of two images. We notice that MROA obtains more competitive results than others from these results. MROA produces better results at all threshold levels for image 1, image 2, image 5, and image 8, respectively. While for image 4, image 6, and image 7, MROA outperforms others at three levels. For image 3, MROA only provides high accuracy for image 3 at two levels.

Figure 14 summarizes the number of best cases obtained by algorithms in terms of fitness, *PSNR*, *SSIM*, and *FSIM*. According to this figure, MROA is significantly improved upon its original. AO and GWO are ranked second and third, respectively.

Table A7 shows the *p*-value obtained by algorithms using the Wilcoxon rank-sum test with a 5% significance level. According to this table, we can see that MROA produces statistically significant results compared with other algorithms. Especially when compared with RSA, AOA, and SCA, MROA has a significant difference between them, which indicates MROA has been improved considerably.

Table A8 shows the CPU time of each algorithm under different thresholds. As it is possible to observe, in most cases a shorter time is obtained using RSA, AOA, and SCA, respectively. However, as shown in Tables A3–A6, RSA, AOA, and SCA may not produce threshold values for segmenting given images well. For the proposed MROA, although MROA increases the CPU time over its original when segmenting images, considering the NFL theorem, it is acceptable to increase some CPU time cost to obtain a better solution.

Overall, the proposed method, MROA, can obtain higher fitness, *PSNR*, *SSIM*, and *FSIM* for most images at different levels, showing that the MROA-based multi-level thresholding segmentation technique can obtain better evaluation results, which further indicates that it can better perform the segmentation of complex grayscale images. It is significantly improved upon the basic version of ROA. Second, it also shows significantly superior performance in terms of fitness, *PSNR*, *SSIM*, and *FSIM* compared with other selected well-known algorithms. It is an excellent approach for solving multi-level thresholding image segmentation, as the BM and LOBL strategies significantly enhance the performance of ROA in determining the optimal threshold values, exhibiting excellent searchability and jumping out of the local optimal solution when solving multi-level thresholding segmentation tasks, and we will apply it to handle other datasets such as medical images, remote sensing images, etc.

7. Conclusions and Future Works

This paper introduces a modified remora optimization algorithm, namely MROA, for global optimization and multi-level thresholding image segmentation tasks. The original ROA has some fatal issues such as premature convergence and easy stagnation into local optimal solutions, which means it cannot solve complex real-world problems. In this work, Brownian motion improves the ROA's exploration ability and provides a higher opportunity to find the optimal or near-optimal solution in the search space. Second, the Lens opposition-based learning enhances the exploitation capability and promotes search agents to jump out the local optimal solution.

We first evaluate the optimization performance of the proposed MROA using 23 benchmark functions. The experimental results demonstrate that MROA has broader searchability and a greater opportunity to obtain high-quality solutions than the original ROA. In addition, based on the analysis and comparison of MROA with other well-known MAs, it can be seen that MROA also has a better overall ability than its peers in optimization accuracy, convergence speed, and significant difference. Therefore, we consider that MROA is an excellent meta-heuristic for function optimization.

Subsequently, the MROA is applied to solve multi-level thresholding image segmentation tasks and obtain optimal threshold values by cross-entropy. The performance of the proposed work is also compared with its peers. Experimental evaluation metrics including *PSNR*, *SSIM*, *FSIM* are used to test the segmented image quality. Furthermore, a statistical test is used to evaluate the significant difference between the two methods. Experimental results proved the following: (1) the MROA significantly improves the original ROA's performance for the image thresholding segmentation task. (2) MROA produces excellent results in terms of *PSNR*, *SSIM*, and *FSIM* compared with the other compared MAs. (3) Wilcoxon rank-sum results indicate that MROA produces a significant performance compared with other selected MAs. Finally, we conclude that the proposed MROA can generate

high-quality segmented images, outperforms other selected MAs in terms of segmentation accuracy, and is more stable and promising.

While the proposed MROA has significant improvements over the original ROA and shows excellent results compared with other selected MAs in terms of benchmark function optimization and image segmentation, the CPU time also increases when solving the image segmentation task. In the future, we will: (1) Reduce the CPU time without degrading MROA's performance; we can design a new effective strategy or hybrid the proposed method with other MAs. (2) Extend the image dataset to include images such as medical images and remote sensing images and increase threshold values to further prove the performance of MROA. (3) Since MROA is a high-performance optimizer, MROA must be applied in other fields such as feature selection, engineering design problems, and maximum power point tracking.

Author Contributions: Q.L., Conceptualization, methodology, software, formal analysis, investigation, data curation, visualization, writing-original draft preparation, funding acquisition. N.L., conceptualization, methodology, resources, review and editing, supervision, funding acquisition. H.J., conceptualization, supervision, methodology, review and editing, funding acquisition. Q.Q., supervision, methodology, review and editing, funding acquisition. L.A., review and editing, supervision. All authors have read and agreed to the published version of the manuscript.

Funding: This research was funded by the Innovative Research Project for Graduate Students of Hainan Province under grant No. Qhys2021-190, the Natural Science Foundation Project of Hainan Province for High Level Talents under grant No. 621RC511, the National Natural Science Foundation of China under grant No. 11861030, the National Key Research and Development Program of China under grant No. 2018YFB1404400, the Natural Science Foundation of Hainan Province under grant No. 2019RC176, the Natural Science Foundation of Fujian Province under grant No. 2021J011128, the Sanming University National Natural Science Foundation Breeding Project under grant No. PYT2105, and the Sanming University Introduces High Level Talents to Start Scientific Research Funding Support Project under grant No. 20YG14.

Institutional Review Board Statement: Not applicable.

Informed Consent Statement: Not applicable.

Data Availability Statement: The data presented in this study are available on request from the corresponding authors.

Conflicts of Interest: The authors declare no conflict of interest.

Appendix A

Table A1. The best threshold values obtained by algorithms over all images.

Image	nTh	MROA	ROA	RSA	AOA	AO	SSA	SCA	GWO
Image 1	4	48 84 123 176	48 84 123 176	47 72 113 158	60 88 144 210	48 84 123 176	48 84 123 176	45 76 119 167	48 84 123 176
	8	34 52 73 94	34 52 73 94	6 8 28 42 61	29 54 80 93	34 52 73 94	35 53 74 95	37 54 69 100	34 52 73 94
		115 138 164 201	115 138 164 201	104 132 195	102 138 211 243	115 138 164 201	116 139 166 202	116 131 163 191	115 138 164 201
	12	29 40 53 68	30 41 54 68	39 59 63 82	30 39 43 48	29 40 53 68	29 40 53 68	1 9 26 42	23 33 45 59
		82 96 111 126	83 97 111 126	88 101 103 115	77 99 111 125	83 97 111 126	82 96 111 127	51 63 84 102	74 90 105 121
		143 162 187 216	143 162 187 216	144 175 199 225	159 199 210 245	142 162 187 216	144 164 190 218	113 138 168 191	138 157 182 212
	16	27 35 44 54	13 28 37 47	12 12 13 22	12 27 41 53	27 35 44 54	26 34 43 54	15 22 23 33	2 3 28 37
		65 76 87 97	58 70 82 93	31 42 59 74	67 71 79 92	65 76 87 98	66 78 90 102	46 61 73 92	47 58 70 83
		108 119 131 144	105 117 130 143	82 94 105 115	109 120 137 139	110 122 136 148	114 127 141 156	110 119 140 161	95 108 121 135
		159 177 199 223	158 176 198 222	124 150 173 209	149 167 191 254	162 179 200 223	173 193 213 232	181 212 227 231	151 170 194 220
Image 2	4	58 88 141 196	58 88 141 196	43 75 126 175	64 81 144 193	58 88 141 196	58 88 141 196	55 87 144 197	58 88 141 196
	8	47 61 78 99	46 60 76 98	46 72 97 113	53 79 122 166	47 62 81 103	46 60 77 98	10 48 61 84	47 61 78 99
		126 162 193 220	124 157 191 221	118 160 200 235	174 192 200 219	130 165 193 218	125 161 192 219	106 149 185 207	126 162 193 220
	12	43 53 63 75	43 53 63 75	9 32 40 44	13 27 42 61	43 53 63 75	45 57 69 83	10 37 48 65	1 45 57 69
		89 104 122 146	90 105 124 148	58 76 92 104	78 94 117 141	87 102 118 139	100 119 140 163	88 99 109 128	83 100 119 143
		170 190 207 231	172 190 208 231	132 158 200 215	143 164 198 218	165 190 209 233	183 197 212 234	132 153 189 214	168 189 207 231
	16	40 48 56 64	41 50 59 68	4 13 19 38	21 31 45 59	16 42 51 60	5 40 48 56	4 30 43 55	2 37 44 51
		73 84 96 107	80 92 105 119	44 52 58 67	64 75 76 95	69 81 94 107	64 73 84 96	65 75 83 86	57 65 74 86
		120 137 156 174	134 152 167 181	74 86 103 121	129 143 164 193	123 143 164 179	108 122 141 162	106 134 160 187	98 110 126 147
		189 202 216 236	192 204 217 236	147 151 191 222	200 213 246 247	191 202 216 235	184 199 215 238	191 213 217 229	171 191 208 231
Image 3	4	60 90 129 175	60 90 129 175	60 90 129 175	63 84 137 169	60 90 129 175	60 90 129 175	60 90 124 176	60 90 129 175
	8	46 62 79 98	46 62 79 98	45 62 79 98	41 51 57 85	46 62 79 98	46 62 80 100	40 51 67 82	45 62 79 98
		121 143 159 188	120 142 159 188	120 142 159 188	117 141 198 225	120 142 159 188	123 146 165 202	89 125 149 172	120 142 159 188
	12	40 52 63 75	41 53 64 76	10 23 30 50	8 28 55 66	40 52 64 75	40 52 63 75	32 51 58 70	38 49 59 70
		87 100 115 131	88 101 116 132	64 67 85 103	74 88 98 112	87 101 116 131	87 100 115 131	79 97 107 128	82 95 110 127
		146 158 172 199	146 158 172 199	125 139 165 188	141 169 186 203	145 157 170 197	146 159 176 208	145 175 211 255	144 157 171 198
	16	37 46 55 63	32 40 50 58	1 20 33 39	20 34 52 68	12 38 47 56	17 40 51 61	1 2 40 59	36 43 50 58
		72 81 90 100	67 76 85 96	43 57 61 73	76 78 82 93	65 74 83 93	72 83 96 110	65 72 82 92	65 73 82 92
		110 122 134 145	107 120 134 145	75 95 115 124	105 118 142 153	105 119 132 144	127 143 154 164	97 104 119 140	102 114 127 139
		154 163 177 203	154 163 177 203	147 155 161 206	188 200 238 245	154 164 182 208	179 199 218 242	161 178 193 255	149 159 173 200

Table A1. *Cont.*

Image	nTh	MROA	ROA	RSA	AOA	AO	SSA	SCA	GWO
Image 4	4	35 66 97 137	35 66 97 137	20 57 91 127	31 60 114 131	35 66 97 137	35 66 97 137	34 65 93 134	35 66 97 137
	8	23 42 61 77	23 42 61 77	4 15 23 48	39 62 72 100	23 42 61 77	23 42 61 77	17 30 51 70	23 42 61 77
		94 114 137 168	94 114 137 168	63 87 109 151	110 124 149 179	93 113 136 167	94 114 137 168	94 122 155 188	94 114 137 168
	12	18 29 42 55	17 27 40 53	11 19 24 31	20 29 51 62	17 27 39 51	22 39 54 68	1 2 12 17	17 28 41 54
		66 77 89 102	65 77 89 102	49 55 60 70	92 104 117 125	63 74 85 98	81 94 110 128	33 51 66 84	65 76 88 101
		117 133 150 175	117 133 150 175	96 113 129 157	151 168 183 232	113 129 149 175	146 168 193 226	99 111 145 168	116 132 149 174
	16	14 21 30 39	15 23 32 42	8 9 21 24	1 10 23 32	13 21 29 39	14 21 31 42	1 1 1 5	8 15 23 32
		49 58 67 75	52 61 69 77	42 43 55 56	34 50 59 76	49 58 67 75	53 63 73 83	15 20 27 32	42 53 63 73
		84 93 105 118	85 94 105 118	60 69 85 99	83 105 120 127	84 93 105 117	95 108 122 138	45 60 74 90	82 92 104 118
		132 147 166 188	132 147 166 188	119 128 144 157	161 188 206 247	131 147 164 185	153 172 189 205	98 119 150 167	132 147 166 188
Image 5	4	31 71 118 171	31 71 118 171	26 48 89 144	35 95 137 175	31 71 118 171	31 71 118 171	30 72 118 178	31 71 118 171
	8	18 33 54 78	18 33 54 78	18 26 41 47	25 60 97 114	18 34 56 81	20 38 62 89	23 39 51 71	20 38 62 88
		104 132 163 206	104 132 163 206	71 100 130 172	124 151 167 189	107 135 166 208	116 143 173 215	98 121 160 216	115 143 173 214
	12	15 24 37 52	14 23 36 52	12 16 30 38	14 25 43 64	15 24 36 51	15 25 39 55	10 14 20 35	15 25 39 55
		69 87 105 123	69 87 105 123	40 52 76 108	103 105 132 162	66 83 101 120	73 92 111 129	51 65 91 116	72 89 106 124
		142 162 186 221	142 162 186 221	113 158 181 228	169 194 235 255	140 161 186 222	149 171 196 230	127 151 189 220	143 163 187 222
	16	13 19 27 37	10 15 21 30	5 9 16 24	3 15 26 42	13 19 28 39	14 22 34 49	1 9 15 26	10 14 19 26
		49 61 74 87	41 53 66 80	38 52 54 75	71 71 97 121	52 64 78 92	64 78 93 107	26 40 53 65	34 44 56 70
		101 114 128 143	94 109 124 139	81 83 89 98	142 176 187 190	105 117 130 143	121 135 150 165	88 116 140 144	84 99 115 131
		158 175 195 226	155 173 194 225	105 131 151 196	224 236 240 250	158 174 194 224	180 197 218 235	163 178 198 236	149 168 190 223
Image 6	4	52 91 139 181	52 91 139 181	31 59 101 161	49 74 113 178	52 91 139 181	52 91 139 181	54 90 134 174	52 91 139 181
	8	35 53 75 102	34 51 72 99	6 42 55 65	36 67 87 105	35 53 74 100	34 50 71 98	32 51 79 104	36 53 75 102
		131 159 183 198	129 157 182 198	95 114 158 188	137 186 195 212	129 157 182 198	128 157 182 198	137 176 198 199	131 159 183 198
	12	29 40 52 67	30 41 53 68	23 36 37 40	28 32 44 59	32 45 59 77	31 44 58 77	1 3 41 49	29 38 49 62
		84 104 125 146	85 105 126 146	50 52 70 106	66 99 102 136	98 117 137 156	97 117 139 160	69 88 118 144	79 99 120 141
		166 183 195 203	166 183 195 203	128 158 187 194	145 177 178 199	172 185 195 203	179 191 200 210	167 172 194 204	162 181 194 202
	16	26 35 44 53	25 34 42 50	30 41 61 63	25 32 40 46	29 38 48 61	25 33 41 49	1 13 26 34	9 11 27 37
		64 76 91 107	60 70 84 99	79 91 112 122	68 68 97 119	76 91 106 119	59 71 86 101	45 52 72 90	46 57 70 84
		123 140 156 171	116 131 147 162	146 164 176 189	127 129 149 152	130 141 152 164	118 135 154 170	90 116 142 159	101 118 137 156
		184 193 199 205	175 187 196 203	196 228 245 254	180 182 183 201	176 187 196 203	184 194 200 206	180 186 198 238	172 186 196 203

Table A1. *Cont.*

Image	nTh	MROA	ROA	RSA	AOA	AO	SSA	SCA	GWO
Image 7	4	55 82 113 149	55 82 113 149	40 60 90 124	54 90 142 182	55 82 113 149	55 82 113 149	52 76 109 142	55 82 113 149
	8	43 58 73 88	43 58 73 88	5 43 60 62	6 46 79 90	43 58 73 88	44 59 74 89	3 46 67 86	43 58 73 87
		106 127 148 169	106 127 148 169	85 89 119 148	116 133 153 183	106 127 148 169	107 128 149 170	95 121 150 176	104 125 147 168
	12	39 49 59 69	39 49 59 69	23 36 37 39	52 72 94 103	39 49 60 71	41 53 65 76	1 2 32 39	39 48 58 68
		78 88 99 112	78 88 99 113	51 61 71 81	112 123 138 142	80 90 101 114	87 100 116 133	51 64 69 86	78 88 99 113
		127 141 156 175	127 141 156 175	99 114 140 150	154 174 195 201	128 143 157 176	150 166 187 248	109 137 160 185	128 142 157 175
	16	37 44 52 60	37 45 53 61	14 18 28 36	11 45 46 54	37 45 53 61	2 39 49 59	1 1 2 38	12 15 38 47
		68 75 82 90	69 77 84 93	49 56 64 65	58 60 67 84	69 76 83 91	68 77 86 96	51 60 74 90	56 65 74 83
		99 109 121 132	103 114 126 137	78 83 107 129	98 114 129 153	98 107 118 130	107 118 130 142	97 114 124 145	92 102 114 127
		143 155 168 185	148 159 170 186	146 150 168 210	181 189 209 235	142 155 169 186	154 167 183 212	156 181 213 238	140 153 166 183
Image 8	4	47 93 115 132	47 93 115 132	43 65 99 122	54 112 130 159	47 93 115 132	47 93 115 132	38 78 113 130	47 93 115 132
	8	18 37 66 94	17 35 64 93	11 17 50 61	12 25 68 108	18 39 69 94	18 37 66 94	3 16 33 64	18 34 59 84
		110 121 130 140	110 121 130 140	81 97 121 134	119 134 161 236	111 122 131 140	112 125 137 237	96 98 114 132	100 114 126 137
	12	15 25 38 58	15 26 39 60	4 16 20 27	12 26 44 58	16 26 38 58	16 29 48 72	1 7 13 15	17 26 38 59
		78 93 104 113	80 93 104 113	32 63 74 75	84 97 103 120	78 92 103 112	90 102 113 122	16 31 62 87	78 92 103 112
		121 128 134 142	121 128 134 142	90 100 114 131	134 134 230 235	121 129 136 143	129 136 143 197	104 117 128 134	120 127 133 141
	16	14 23 31 44	13 20 27 35	10 14 17 21	15 37 66 68	12 18 25 30	14 24 36 55	1 1 1 10	4 13 20 27
		60 75 85 94	47 62 78 89	28 34 39 47	71 95 97 110	36 44 53 69	74 87 98 109	14 18 27 41	37 54 70 82
		103 110 116 122	98 106 113 120	50 67 81 93	116 126 137 144	84 97 107 115	117 124 132 141	62 81 91 103	93 103 112 119
		127 132 138 145	126 131 137 144	111 120 135 177	161 181 210 233	123 130 137 144	202 233 248 253	107 120 128 135	125 131 137 144

Table A2. The segmented images obtained by MROA using cross-entropy.

Image	nTh = 4	nTh = 8	nTh = 12	nTh = 16
Image 1	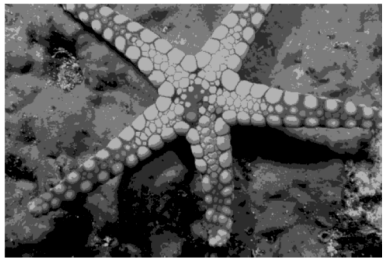	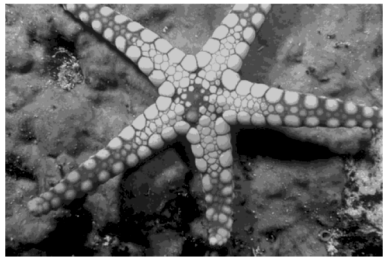	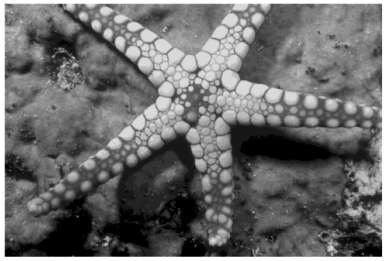	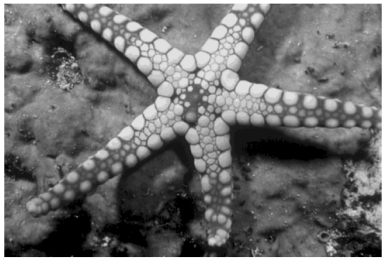

Table A2. *Cont.*

Image	nTh = 4	nTh = 8	nTh = 12	nTh = 16
Image 2	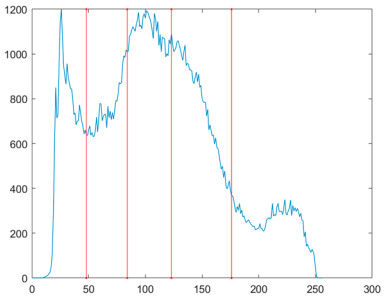  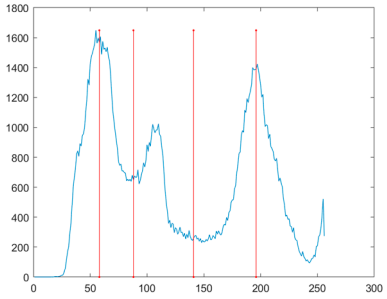	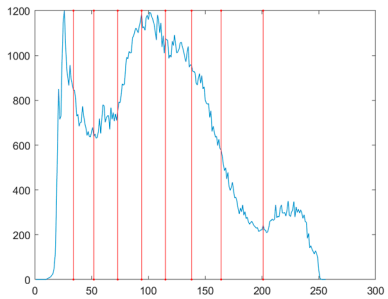  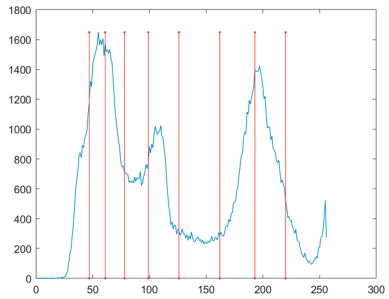	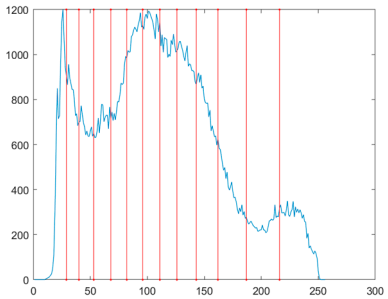  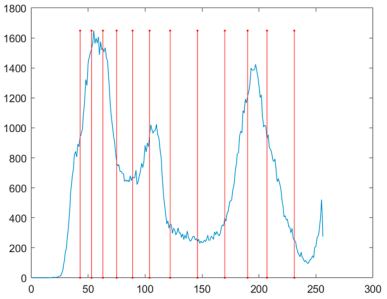	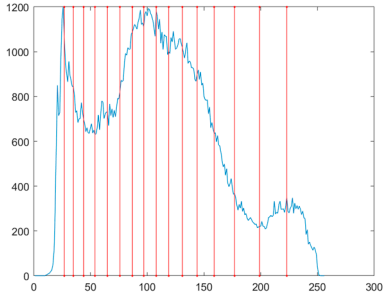  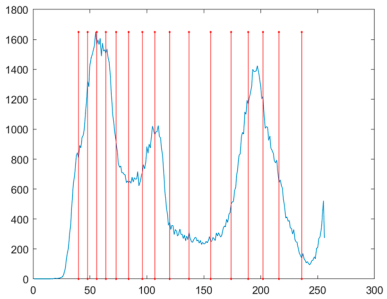

Table A2. *Cont.*

Image	nTh = 4	nTh = 8	nTh = 12	nTh = 16
Image 3	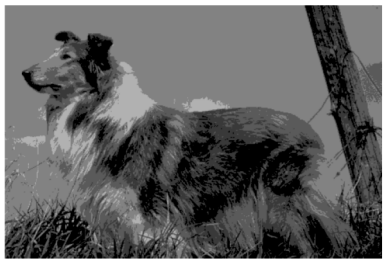 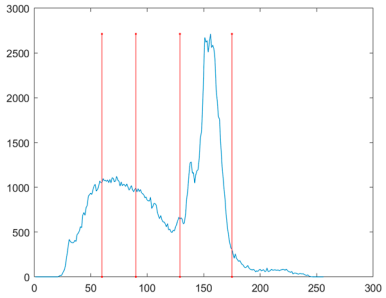	 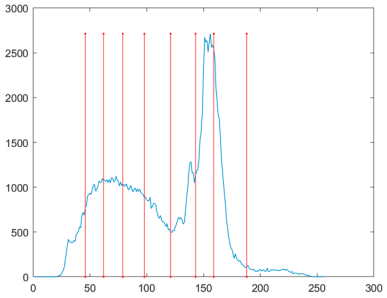	 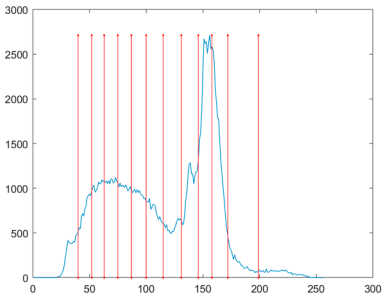	 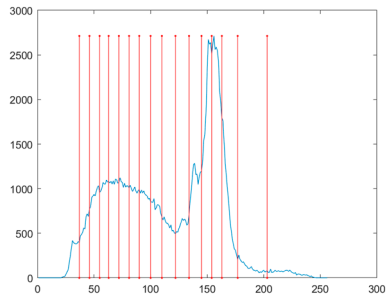
Image 4				

Table A2. *Cont.*

Image	nTh = 4	nTh = 8	nTh = 12	nTh = 16
Image 5	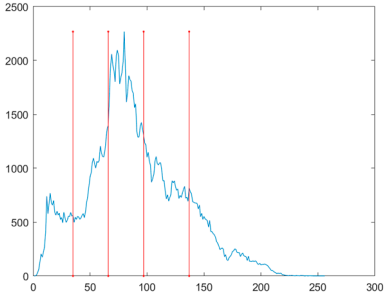	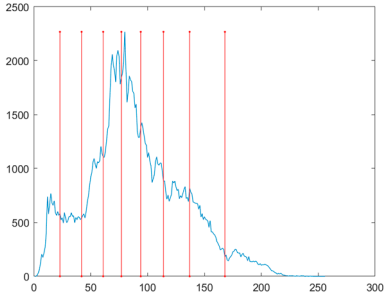	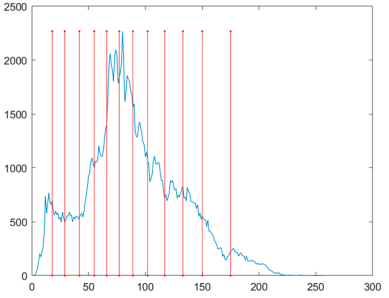	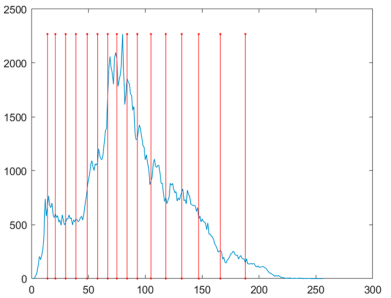
				
	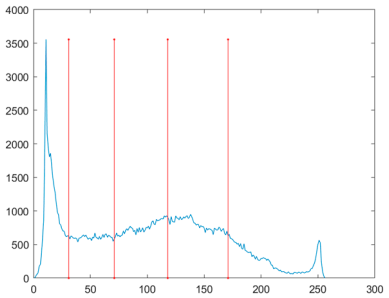	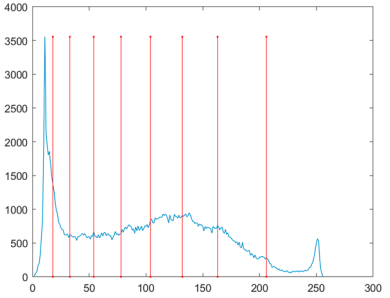	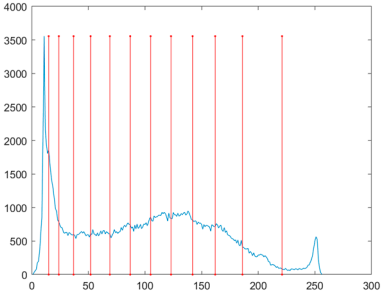	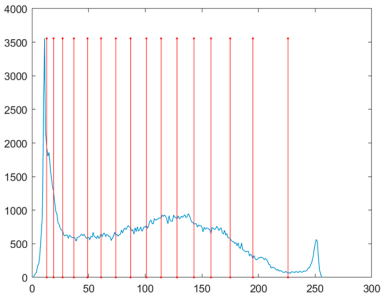

Table A2. *Cont.*

Image	nTh = 4	nTh = 8	nTh = 12	nTh = 16
Image 6				
	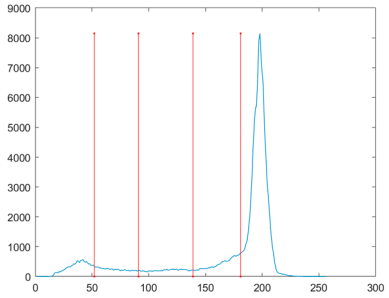	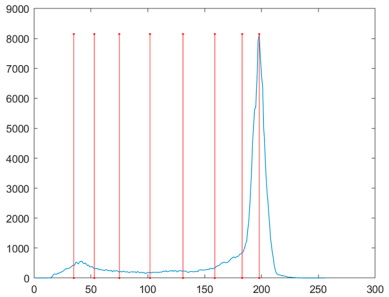	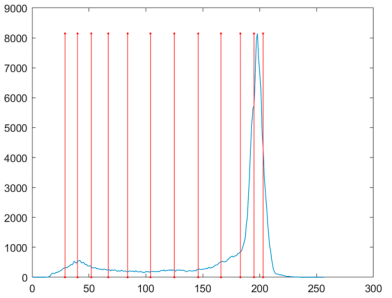	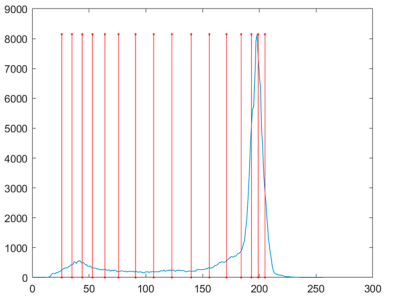
Image 7				

Table A2. *Cont.*

Image	nTh = 4	nTh = 8	nTh = 12	nTh = 16
Image 8	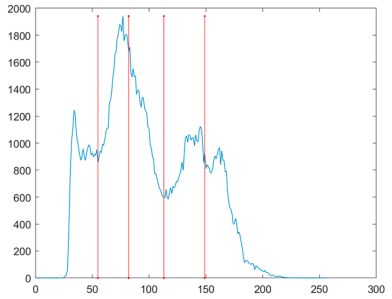	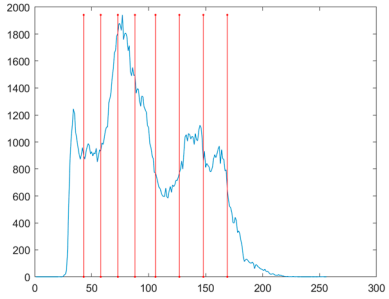	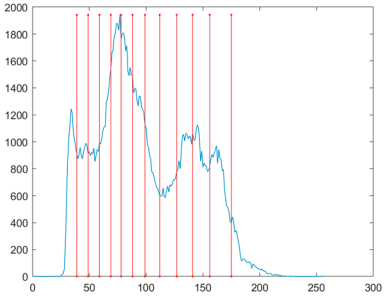	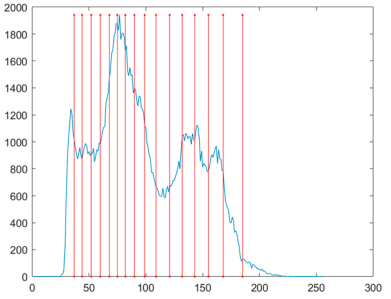
				
	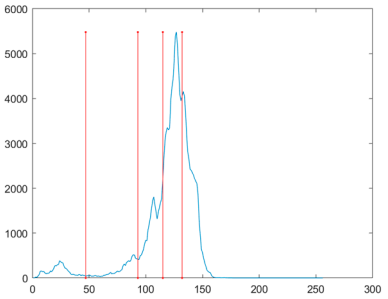	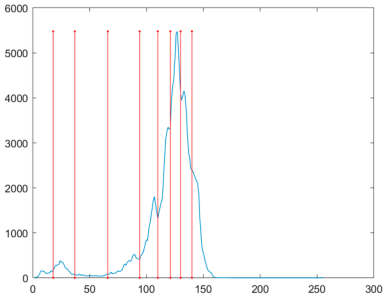	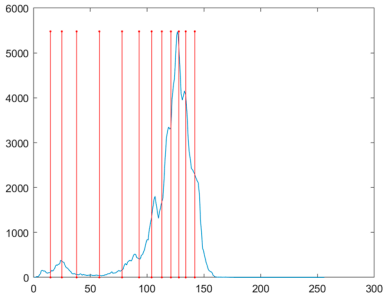	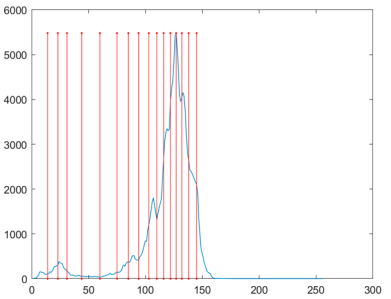

Table A3. The best fitness values obtained by algorithms over all images.

Image	nTh	MROA		ROA		RSA		AOA		AO		SSA		SCA		GWO	
		Mean	**Std**	**Mean**	**Std**	**Mean**	**Std**	**Mean**	**Std**	**Mean**	**Std**	**Mean**	**Std**	**Mean**	**Std**	**Mean**	**Std**
Image 1	4	**0.7841**	0	**0.7841**	0	1.0771	0.1565	1.1233	0.1872	**0.7841**	0	**0.7841**	0	0.8220	0.0821	**0.7841**	0
	8	**0.2429**	0	**0.2429**	0	0.4622	0.0690	0.4836	0.0737	**0.2429**	0	0.2430	0.0001	0.3723	0.0476	**0.2429**	0
	12	**0.1207**	0.0037	0.1213	0.0050	0.2567	0.0372	0.2878	0.0553	0.1222	0.0064	0.1282	0.0081	0.2268	0.0364	0.1337	0.0144
	16	**0.0713**	0.0016	0.0744	0.0049	0.1760	0.0227	0.1784	0.0269	0.0731	0.0048	0.0841	0.0097	0.1659	0.0239	0.0814	0.0096
Image 2	4	**0.6216**	0	**0.6216**	0	0.7838	0.0836	0.8572	0.0885	**0.6216**	0	**0.6216**	0	0.6389	0.0084	**0.6216**	0
	8	**0.2052**	0.0107	0.2075	0.0149	0.3799	0.0578	0.3868	0.0520	0.2054	0.0107	0.2081	0.0121	0.3064	0.0381	0.2091	0.0179
	12	0.1006	0.0063	**0.0988**	0.0033	0.2058	0.0266	0.2152	0.0350	0.1019	0.0085	0.1060	0.0078	0.1970	0.0185	0.1118	0.0116
	16	**0.0586**	0.0021	0.0622	0.0052	0.1476	0.0207	0.1499	0.0249	0.0640	0.0076	0.0666	0.0042	0.1340	0.0155	0.0736	0.0085
Image 3	4	**0.5146**	0	**0.5146**	0	0.6802	0.0779	0.7292	0.1052	**0.5146**	0	**0.5146**	0	0.5276	0.0070	**0.5146**	0
	8	**0.1609**	0	0.1678	0.0157	0.3159	0.0545	0.3688	0.0522	0.1625	0.0076	0.1676	0.0142	0.2528	0.0470	0.1679	0.0157
	12	**0.0788**	0.0037	0.0798	0.0065	0.1866	0.0346	0.2186	0.0367	0.0806	0.0068	0.0927	0.0109	0.1659	0.0225	0.0894	0.0084
	16	**0.0462**	0.0015	0.0481	0.0064	0.1322	0.0158	0.1439	0.0267	0.0490	0.0047	0.0631	0.0093	0.1207	0.0167	0.0585	0.0050
Image 4	4	**0.7421**	0	**0.7421**	0	1.0030	0.1326	1.1431	0.1646	0.7421	0	**0.7421**	0	0.7580	0.0104	**0.7421**	0
	8	**0.2332**	0	**0.2332**	0	0.4483	0.0561	0.5239	0.1076	0.2332	0.0001	0.2568	0.0360	0.3632	0.0557	0.2352	0.0104
	12	**0.1179**	0.0002	0.1180	0.0003	0.2714	0.0429	0.3157	0.0489	0.1191	0.0034	0.1517	0.0171	0.2348	0.0329	0.1243	0.0081
	16	**0.0699**	0.0004	0.0707	0.0022	0.1846	0.0293	0.2172	0.0389	0.0711	0.0020	0.1022	0.0096	0.1754	0.0244	0.0795	0.0057
Image 5	4	**1.1119**	0	**1.1119**	0	1.3808	0.1714	1.5084	0.2439	**1.1119**	0	**1.1119**	0	1.1324	0.0128	**1.1119**	0
	8	0.3530	0.0003	**0.3529**	0.0002	0.5602	0.0859	0.6133	0.0756	0.3533	0.0004	0.3539	0.0004	0.4862	0.0550	0.3563	0.0158
	12	**0.1639**	0.0001	0.1648	0.0051	0.3297	0.0348	0.3819	0.0345	0.1647	0.0009	0.1811	0.0134	0.3013	0.0356	0.1708	0.0110
	16	**0.0974**	0.0002	0.0977	0.0013	0.2304	0.0352	0.2394	0.0347	0.0987	0.0013	0.1145	0.0087	0.2093	0.0256	0.1074	0.0076
Image 6	4	**0.3155**	0	**0.3155**	0	0.4261	0.0831	0.4697	0.0487	**0.3155**	0	**0.3155**	0	0.3284	0.0063	**0.3155**	0
	8	**0.1135**	0	0.1145	0.0054	0.1980	0.0208	0.2238	0.0360	0.1167	0.0090	0.1167	0.0093	0.1701	0.0154	0.1136	0.0001
	12	**0.0583**	0.0001	0.0616	0.0054	0.1283	0.0190	0.1345	0.0212	0.0613	0.0038	0.0646	0.0045	0.1175	0.0154	0.0657	0.0055
	16	**0.0353**	0.0003	0.0363	0.0023	0.0911	0.0121	0.0919	0.0131	0.0387	0.0033	0.0418	0.0028	0.0838	0.0102	0.0426	0.0040
Image 7	4	**0.4359**	0	**0.4359**	0	0.7059	0.1129	0.7571	0.1361	**0.4359**	0	**0.4359**	0	0.4796	0.0709	**0.4359**	0
	8	**0.1500**	0.0065	0.1560	0.0146	0.3189	0.0433	0.3656	0.0734	0.1536	0.0124	0.1600	0.0169	0.2452	0.0381	0.1550	0.0135
	12	**0.0731**	0.0021	0.0797	0.0088	0.2030	0.0325	0.2301	0.0403	0.0741	0.0034	0.0910	0.0077	0.1661	0.0262	0.0833	0.0083
	16	**0.0435**	0.0022	0.0458	0.0039	0.1344	0.0215	0.1487	0.0265	0.0476	0.0069	0.0712	0.0104	0.1244	0.0221	0.0552	0.0059
Image 8	4	**0.2223**	0	**0.2223**	0	0.3345	0.0525	0.3855	0.0672	**0.2223**	0	**0.2223**	0	0.2471	0.0318	**0.2223**	0
	8	**0.0773**	0.0015	0.0776	0.0016	0.1744	0.0327	0.1959	0.0372	0.0832	0.0072	0.1008	0.0181	0.1431	0.0253	0.0802	0.0098
	12	**0.0390**	0.0013	0.0395	0.0026	0.1121	0.0204	0.1243	0.0181	0.0470	0.0059	0.0591	0.0092	0.1001	0.0151	0.0433	0.0039
	16	**0.0238**	0.0005	0.0241	0.0012	0.0782	0.0136	0.0921	0.0197	0.0306	0.0037	0.0395	0.0060	0.0721	0.0133	0.0300	0.0039

Table A4. The *PSNR* values obtained by algorithms over all images.

Image	nTh	MROA		ROA		RSA		AOA		AO		SSA		SCA		GWO	
		Mean	**Std**	**Mean**	**Std**	**Mean**	**Std**	**Mean**	**Std**	**Mean**	**Std**	**Mean**	**Std**	**Mean**	**Std**	**Mean**	**Std**
Image 1	4	**19.3376**	0	**19.3376**	0	18.3018	0.5249	18.1087	0.7026	**19.3376**	0	**19.3376**	0	19.2121	0.3509	**19.3376**	0
	8	**24.1491**	0.0004	24.1163	0.1022	21.7778	0.7749	21.7991	0.7920	24.1475	0.0117	24.1281	0.0254	22.7241	0.6679	24.1208	0.0330
	12	**27.1246**	0.0506	27.1175	0.1278	24.5001	0.8100	24.2200	0.9564	27.0969	0.1278	27.0828	0.2336	25.0032	0.8174	26.9968	0.2814
	16	**29.3117**	0.3068	29.1876	0.1377	26.1545	0.7347	26.2696	0.8709	29.1290	0.1958	28.9716	0.4423	26.4606	0.8718	29.2671	0.4458
Image 2	4	**18.0038**	0	**18.0038**	0	17.3395	1.0346	16.6057	0.8798	**18.0038**	0	**18.0038**	0	17.8871	0.4044	**18.0038**	0
	8	22.9234	0.2940	22.9831	0.2279	21.4067	0.9250	20.7784	1.4500	22.9835	0.1557	22.9421	0.2441	21.9460	1.0323	**23.0198**	0
	12	**26.2492**	0.8132	25.9659	0.0706	24.1938	0.9844	24.3899	1.0967	25.9085	0.2792	26.1072	0.5823	24.5498	0.9768	25.9665	0.1556
	16	**28.6702**	0.9003	28.5102	0.4960	26.0587	1.0591	25.9470	1.5180	28.0976	0.5281	28.5808	0.9061	26.1646	1.1019	28.2240	0.3534
Image 3	4	**19.2818**	0	**19.2818**	0	19.6628	1.0716	18.3815	1.3124	**19.2818**	0	**19.2818**	0	19.3864	0.4334	**19.2818**	0
	8	25.0831	0.1982	**25.1037**	0.1279	23.1708	0.9900	22.1617	1.5444	25.0772	0.1405	25.0645	0.2753	23.8852	1.1119	25.0825	0.0498
	12	**28.3161**	0.3359	28.3135	0.1234	25.9299	1.0497	25.0463	1.2403	28.2351	0.2469	27.9632	0.6398	26.0484	1.0511	28.2085	0.1756
	16	**30.7671**	0.5883	30.4644	0.3260	27.5699	0.8206	26.6435	1.4561	30.3897	0.2585	30.0481	0.7364	27.6447	1.0729	30.3287	0.2183
Image 4	4	**21.5871**	0	**21.5871**	0	20.0717	0.6269	19.6025	0.7700	**21.5871**	0	21.5873	0.0015	21.4809	0.1121	**21.5871**	0
	8	**26.5589**	0.0069	**26.5589**	0.0069	23.5589	0.5653	23.0839	0.9430	26.5571	0.0112	26.1229	0.6104	24.6063	0.6936	26.5122	0.1869
	12	**29.6429**	0.0275	29.6386	0.0264	25.6695	0.7268	25.4587	0.7456	29.5274	0.1877	28.6563	0.4896	26.5354	0.6833	29.3460	0.2953
	16	31.8382	0.0452	31.8289	0.0953	27.2667	0.6992	27.1155	0.9276	**31.8484**	0.1858	30.5278	0.4131	27.9195	0.7135	31.3087	0.3760
Image 5	4	**19.2461**	0	**19.2461**	0	17.9538	0.6767	18.1794	0.7934	**19.2461**	0	**19.2461**	0	19.1712	0.1436	**19.2461**	0
	8	23.9514	0.0931	23.8599	0.0533	21.8629	0.8876	21.8907	0.6947	23.9489	0.1324	**24.1104**	0.1092	22.7269	0.4555	23.8973	0.1859
	12	27.2929	0.0189	27.2513	0.1417	24.0802	0.6301	24.2450	0.6203	27.1837	0.1124	**27.3553**	0.1605	24.6915	0.5420	27.0084	0.2825
	16	29.4540	0.0650	29.4478	0.0520	25.5730	0.7455	25.9613	0.8057	29.3635	0.1642	**29.4927**	0.2483	26.2597	0.7296	29.0170	0.3157
Image 6	4	**21.3607**	0	**21.3607**	0	18.1814	1.8732	19.2881	1.6304	**21.3607**	0	**21.3607**	0	21.0657	0.5319	**21.3607**	0
	8	**26.7272**	0.0939	26.6653	0.1881	22.9715	1.3210	22.9515	1.4407	26.5535	0.3486	26.6476	0.3186	24.7693	1.0491	26.6911	0.0932
	12	**30.1561**	0.0928	30.0108	0.3028	26.1309	1.2163	26.2053	1.4103	29.9128	0.3887	29.8247	0.3918	26.3476	1.2102	29.7359	0.4487
	16	**32.7456**	0.1698	32.7002	0.2186	27.7064	1.4008	28.2815	1.1492	32.2348	0.6961	31.8480	0.4028	28.3961	1.0373	31.8606	0.5641
Image 7	4	**20.6291**	0	**20.6291**	0	19.7123	0.7668	19.4405	1.1533	**20.6291**	0	**20.6291**	0	20.4534	0.4593	**20.6291**	0
	8	24.9744	0.3290	**25.0648**	0.4643	23.7591	0.7303	22.7988	1.4098	24.9277	0.1978	24.7888	0.5062	23.6155	0.8901	24.9333	0.1963
	12	**27.8778**	0.7934	27.6887	0.6917	26.0448	0.9770	24.7738	1.4939	27.3320	0.3696	26.9412	0.8687	25.9186	1.1009	27.5552	0.7761
	16	**30.1065**	1.0516	29.8779	1.4726	27.9510	0.8191	26.6208	1.7484	29.0573	0.8782	28.7837	1.3487	27.5947	1.4798	29.8787	1.1793
Image 8	4	**25.3640**	0	25.3628	0.0069	22.7034	1.2188	21.2011	1.6455	**25.3640**	0	**25.3640**	0	24.4553	1.0689	**25.3640**	0
	8	**30.4785**	0.1435	30.4755	0.1480	26.0074	1.3326	25.8519	1.0730	30.1259	0.5866	29.0871	0.9423	27.2603	1.1301	30.2703	0.5812
	12	**34.1924**	0.2804	34.1184	0.3478	28.3594	1.1360	28.3050	0.9239	32.9863	0.8048	32.0325	0.8260	28.8706	1.1758	33.4289	0.5617
	16	**36.7245**	0.3031	36.6173	0.4843	29.8648	1.1453	29.6225	1.3039	35.1034	0.6833	33.8346	0.8438	30.8730	1.1133	35.2055	0.7466

Table A5. The SSIM values obtained by algorithms over all images.

Image	nTh	MROA		ROA		RSA		AOA		AO		SSA		SCA		GWO	
		Mean	**Std**	**Mean**	**Std**	**Mean**	**Std**	**Mean**	**Std**	**Mean**	**Std**	**Mean**	**Std**	**Mean**	**Std**	**Mean**	**Std**
Image 1	4	**0.6506**	0	**0.6506**	0	0.6475	0.0198	0.5962	0.0333	**0.6506**	0	**0.6506**	0	0.6448	0.0145	**0.6506**	0
	8	**0.8141**	0.0072	0.8125	0	0.7867	0.0311	0.7421	0.0349	0.8124	0.0002	0.8114	0.0016	0.7801	0.0225	0.8115	0.0014
	12	**0.8863**	0.0091	0.8810	0.0091	0.8542	0.0238	0.8221	0.0352	0.8792	0.0047	0.8711	0.0114	0.8453	0.0260	0.8858	0.0126
	16	0.9179	0.0105	0.9118	0.0033	0.8946	0.0135	0.8652	0.0364	0.9098	0.0033	0.9050	0.0127	0.8871	0.0221	**0.9238**	0.0125
Image 2	4	**0.6249**	0	**0.6249**	0	0.6777	0.0320	0.6010	0.0581	**0.6249**	0	**0.6249**	0	0.6270	0.0209	**0.6249**	0
	8	0.7948	0.0104	0.7969	0.0069	0.7958	0.0298	0.7489	0.0580	0.7966	0.0038	0.7951	0.0082	0.7848	0.0367	**0.7975**	0
	12	**0.8737**	0.0191	0.8678	0.0014	0.8442	0.0335	0.8400	0.0345	0.8659	0.0064	0.8704	0.0142	0.8464	0.0284	0.8678	0.0028
	16	**0.9134**	0.0141	0.9115	0.0075	0.8797	0.0213	0.8703	0.0324	0.9054	0.0087	0.9118	0.0144	0.8774	0.0254	0.9074	0.0056
Image 3	4	0.7280	0	0.7280	0	**0.7700**	0.0276	0.6831	0.0606	0.7280	0	0.7280	0	0.7174	0.0146	0.7280	0
	8	0.8498	0.0025	**0.8514**	0.0069	0.8473	0.0283	0.7856	0.0494	0.8491	0.0021	0.8497	0.0061	0.8347	0.0320	0.8488	0.0011
	12	0.9061	0.0052	**0.9065**	0.0022	0.8819	0.0118	0.8518	0.0309	0.9054	0.0040	0.9000	0.0112	0.8724	0.0225	0.9054	0.0023
	16	**0.9369**	0.0065	0.9345	0.0036	0.9019	0.0138	0.8795	0.0302	0.9332	0.0033	0.9267	0.0087	0.8961	0.0223	0.9324	0.0030
Image 4	4	0.7478	0	0.7478	0	**0.7678**	0.0146	0.7199	0.0327	0.7478	0	0.7478	0	0.7469	0.0085	0.7478	0
	8	**0.8399**	0.0006	**0.8399**	0.0006	0.8327	0.0099	0.7845	0.0229	**0.8391**	0.0005	0.8359	0.0071	0.8253	0.0110	0.8398	0.0008
	12	**0.8914**	0.0010	0.8911	0.0011	0.8604	0.0092	0.8314	0.0193	0.8906	0.0019	0.8704	0.0085	0.8581	0.0131	0.8911	0.0031
	16	**0.9232**	0.0010	0.9230	0.0019	0.8839	0.0094	0.8633	0.0136	0.9228	0.0019	0.8977	0.0072	0.8823	0.0100	0.9215	0.0034
Image 5	4	**0.6850**	0	**0.6850**	0	0.6788	0.0139	0.6360	0.0297	**0.6850**	0	**0.6850**	0	0.6827	0.0040	**0.6850**	0
	8	**0.8219**	0.0012	0.8215	0.0007	0.8076	0.0246	0.7678	0.0288	0.8208	0.0017	0.8190	0.0012	0.8136	0.0191	0.8207	0.0032
	12	**0.8945**	0.0002	0.8871	0.0009	0.8720	0.0219	0.8253	0.0289	0.8865	0.0010	0.8794	0.0069	0.8632	0.0219	0.8908	0.0058
	16	**0.9401**	0.0091	0.9204	0.0019	0.9024	0.0164	0.8723	0.0236	0.9203	0.0014	0.9105	0.0061	0.9045	0.0177	0.9387	0.0123
Image 6	4	0.8741	0	0.8741	0	**0.8858**	0.0110	0.8568	0.0364	0.8741	0	0.8741	0	0.8754	0.0063	0.8741	0
	8	0.8866	0.0015	0.8859	0.0021	**0.9173**	0.0155	0.8801	0.0282	0.8843	0.0047	0.8862	0.0041	0.9028	0.0212	0.8863	0.0013
	12	**0.9206**	0.0014	0.9200	0.0027	0.9159	0.0230	0.8994	0.0225	0.9190	0.0033	0.9174	0.0043	0.9036	0.0230	0.9204	0.0038
	16	**0.9405**	0.0018	0.9401	0.0019	0.9154	0.0197	0.9169	0.0138	0.9376	0.0055	0.9342	0.0036	0.9190	0.0123	0.9359	0.0043
Image 7	4	0.6896	0	0.6896	0	**0.7146**	0.0281	0.6598	0.0524	0.6896	0	0.6896	0	0.6848	0.0117	0.6896	0
	8	0.8237	0.0125	0.8261	0.0170	**0.8352**	0.0235	0.7800	0.0562	0.8214	0.0077	0.8172	0.0155	0.7918	0.0293	0.8220	0.0078
	12	**0.8891**	0.0166	0.8849	0.0143	0.8729	0.0212	0.8261	0.0456	0.8771	0.0074	0.8664	0.0189	0.8507	0.0330	0.8815	0.0155
	16	**0.9214**	0.0149	0.9172	0.0200	0.9022	0.0141	0.8602	0.0403	0.9064	0.0134	0.9004	0.0232	0.8803	0.0321	0.9185	0.0173
Image 8	4	0.8567	0	0.8566	0.0005	**0.8657**	0.0227	0.8352	0.0382	0.8567	0	0.8567	0	0.8468	0.0112	0.8567	0
	8	**0.9113**	0.0032	0.9107	0.0035	0.8871	0.0145	0.8719	0.0166	0.9065	0.0049	0.8973	0.0078	0.8857	0.0106	0.9096	0.0054
	12	**0.9400**	0.0023	0.9395	0.0026	0.9053	0.0136	0.8936	0.0101	0.9303	0.0063	0.9225	0.0068	0.8991	0.0137	0.9349	0.0042
	16	**0.9571**	0.0022	0.9566	0.0031	0.9153	0.0113	0.9096	0.0108	0.9458	0.0048	0.9369	0.0060	0.9193	0.0109	0.9482	0.0049

Table A6. The FSIM values obtained by algorithms over all images.

Image	nTh	MROA		ROA		RSA		AOA		AO		SSA		SCA		GWO	
		Mean	**Std**	**Mean**	**Std**	**Mean**	**Std**	**Mean**	**Std**	**Mean**	**Std**	**Mean**	**Std**	**Mean**	**Std**	**Mean**	**Std**
Image 1	4	**0.7693**	0	**0.7693**	0	0.7333	0.0173	0.7247	0.0219	**0.7693**	0	**0.7693**	0	0.7630	0.0105	**0.7693**	0
	8	**0.8902**	0	0.8895	0.0025	0.8342	0.0184	0.8259	0.0184	0.8902	0.0001	0.8902	0.0003	0.8527	0.0135	0.8901	0.0002
	12	**0.9348**	0.0004	0.9347	0.0014	0.8847	0.0128	0.8736	0.0202	0.9346	0.0018	0.9335	0.0025	0.8943	0.0134	0.9329	0.0034
	16	**0.9548**	0.0025	0.9538	0.0005	0.9129	0.0099	0.9104	0.0127	0.9540	0.0016	0.9535	0.0031	0.9175	0.0112	0.9544	0.0037
Image 2	4	**0.7666**	0	**0.7666**	0	0.7740	0.0137	0.7618	0.0158	**0.7666**	0	**0.7666**	0	0.7705	0.0078	**0.7666**	0
	8	0.8704	0.0026	0.8701	0.0036	0.8410	0.0124	0.8303	0.0209	0.8702	0.0026	0.8704	0.0026	0.8498	0.0154	**0.8707**	0
	12	**0.9211**	0.0064	0.9202	0.0010	0.8858	0.0133	0.8840	0.0151	0.9190	0.0037	0.9205	0.0041	0.8885	0.0137	0.9201	0.0026
	16	**0.9474**	0.0058	0.9461	0.0031	0.9086	0.0135	0.9065	0.0182	0.9432	0.0046	0.9469	0.0054	0.9118	0.0139	0.9449	0.0023
Image 3	4	**0.7903**	0	**0.7903**	0	0.7933	0.0779	0.7529	0.0278	**0.7903**	0	**0.7903**	0	0.7860	0.0049	**0.7903**	0
	8	0.8894	0.0029	**0.8901**	0.0033	0.8692	0.0545	0.8310	0.0276	0.8891	0.0021	0.8891	0.0047	0.8690	0.0223	0.8891	0.0008
	12	0.9314	0.0043	**0.9327**	0.0016	0.9034	0.0346	0.8821	0.0216	0.9317	0.0032	0.9293	0.0076	0.9012	0.0156	0.9315	0.0018
	16	**0.9554**	0.0057	0.9513	0.0028	0.9226	0.0158	0.9076	0.0225	0.9509	0.0025	0.9500	0.0063	0.9221	0.0153	0.9501	0.0021
Image 4	4	**0.7982**	0	**0.7982**	0	0.8032	0.0075	0.7842	0.0131	**0.7982**	0	0.7982	0.0002	0.7991	0.0044	**0.7982**	0
	8	0.8639	0.0001	0.8639	0.0001	0.8371	0.0082	0.8223	0.0146	**0.8640**	0.0003	0.8598	0.0066	0.8431	0.0089	0.8636	0.0016
	12	**0.9055**	0.0004	0.9054	0.0005	0.8630	0.0108	0.8541	0.0100	0.9034	0.0032	0.8902	0.0062	0.8664	0.0085	0.9012	0.0037
	16	**0.9277**	0.0007	0.9274	0.0010	0.8809	0.0087	0.8765	0.0121	0.9274	0.0021	0.9129	0.0055	0.8838	0.0092	0.9253	0.0032
Image 5	4	**0.8264**	0	**0.8264**	0	0.7921	0.0185	0.7861	0.0235	**0.8264**	0	**0.8264**	0	0.8239	0.0033	**0.8264**	0
	8	**0.9063**	0.0024	0.9057	0.0013	0.8750	0.0133	0.8686	0.0157	0.9061	0.0035	0.9116	0.0024	0.8862	0.0089	0.9073	0.0036
	12	**0.9474**	0.0002	0.9471	0.0011	0.9101	0.0085	0.9043	0.0100	0.9468	0.0008	0.9474	0.0020	0.9156	0.0074	0.9457	0.0021
	16	**0.9649**	0.0005	0.9642	0.0009	0.9270	0.0093	0.9258	0.0081	0.9646	0.0009	0.9642	0.0020	0.9362	0.0065	0.9647	0.0024
Image 6	4	**0.8669**	0	**0.8669**	0	0.8631	0.0066	0.8496	0.0135	**0.8669**	0	**0.8669**	0	0.8659	0.0021	**0.8669**	0
	8	0.8903	0.0007	0.8900	0.0009	**0.8924**	0.0071	0.8749	0.0140	0.8897	0.0021	0.8903	0.0018	0.8905	0.0115	0.8903	0.0006
	12	**0.9223**	0.0008	0.9205	0.0034	0.9039	0.0128	0.8945	0.0118	0.9190	0.0039	0.9183	0.0038	0.9010	0.0116	0.9178	0.0037
	16	**0.9397**	0.0010	0.9396	0.0012	0.9127	0.0118	0.9114	0.0092	0.9379	0.0043	0.9350	0.0026	0.9151	0.0085	0.9356	0.0037
Image 7	4	**0.8223**	0	**0.8223**	0	0.8036	0.0113	0.7793	0.0250	**0.8223**	0	**0.8223**	0	0.8116	0.0076	**0.8223**	0
	8	0.8889	0.0036	**0.8902**	0.0051	0.8719	0.0123	0.8483	0.0167	0.8885	0.0015	0.8844	0.0048	0.8685	0.0121	0.8885	0.0021
	12	**0.9226**	0.0077	0.9214	0.0064	0.9005	0.0127	0.8805	0.0176	0.9176	0.0022	0.9154	0.0085	0.8898	0.0115	0.9208	0.0093
	16	**0.9424**	0.0090	0.9421	0.0117	0.9227	0.0094	0.9051	0.0150	0.9343	0.0038	0.9354	0.0111	0.9141	0.0151	0.9411	0.0084
Image 8	4	**0.8587**	0	0.8586	0.0005	0.8623	0.0089	0.8552	0.0120	**0.8587**	0	**0.8587**	0	0.8548	0.0060	**0.8587**	0
	8	**0.8889**	0.0043	0.8879	0.0046	0.8710	0.0096	0.8671	0.0116	0.8835	0.0050	0.8761	0.0058	0.8684	0.0065	0.8871	0.0058
	12	**0.9199**	0.0039	0.9188	0.0039	0.8812	0.0103	0.8774	0.0093	0.9077	0.0078	0.8998	0.0075	0.8779	0.0103	0.9120	0.0059
	16	**0.9446**	0.0034	0.9437	0.0052	0.8900	0.0089	0.8879	0.0098	0.9281	0.0074	0.9159	0.0077	0.8950	0.0103	0.9293	0.0077

Table A7. The *p*-values obtained by algorithms over all images.

Image	nTh	ROA	RSA	AOA	AO	SSA	SCA	GWO
Image 1	4	6.54×10^{-01}	3.15×10^{-12}	3.15×10^{-12}	4.59×10^{-02}	4.59×10^{-01}	3.15×10^{-12}	2.89×10^{-01}
	8	3.34×10^{-01}	1.21×10^{-12}	1.21×10^{-12}	4.19×10^{-02}	4.38×10^{-12}	1.21×10^{-12}	2.89×10^{-05}
	12	7.19×10^{-01}	7.87×10^{-12}	7.87×10^{-12}	2.25×10^{-08}	7.87×10^{-12}	7.87×10^{-12}	1.19×10^{-11}
	16	2.24×10^{-03}	2.92×10^{-11}	2.92×10^{-11}	8.70×10^{-11}	2.92×10^{-11}	2.92×10^{-11}	8.70×10^{-11}
Image 2	4	NaN	1.21×10^{-12}	1.21×10^{-12}	NaN	NaN	1.21×10^{-12}	NaN
	8	1.76×10^{-01}	1.25×10^{-11}	1.25×10^{-11}	2.69×10^{-01}	1.30×10^{-06}	1.25×10^{-11}	4.69×10^{-02}
	12	5.08×10^{-03}	2.37×10^{-11}	2.37×10^{-11}	1.07×10^{-06}	7.87×10^{-11}	2.37×10^{-11}	2.88×10^{-09}
	16	1.80×10^{-02}	3.01×10^{-11}	3.01×10^{-11}	5.48×10^{-11}	3.01×10^{-11}	3.01×10^{-11}	3.01×10^{-11}
Image 3	4	NaN	1.21×10^{-12}	1.21×10^{-12}	NaN	NaN	1.21×10^{-12}	NaN
	8	1.10×10^{-01}	4.10×10^{-12}	4.10×10^{-12}	3.99×10^{-01}	5.00×10^{-08}	4.10×10^{-12}	7.38×10^{-07}
	12	2.30×10^{-01}	2.83×10^{-11}	2.83×10^{-11}	2.42×10^{-05}	9.33×10^{-11}	2.83×10^{-11}	7.65×10^{-11}
	16	5.45×10^{-06}	3.01×10^{-11}	3.01×10^{-11}	2.15×10^{-10}	3.01×10^{-11}	3.01×10^{-11}	3.01×10^{-11}
Image 4	4	NaN	1.21×10^{-12}	1.21×10^{-12}	NaN	NaN	1.21×10^{-12}	NaN
	8	1.98×10^{-02}	1.04×10^{-11}	1.04×10^{-11}	8.90×10^{-01}	1.05×10^{-07}	1.04×10^{-11}	4.98×10^{-02}
	12	4.65×10^{-02}	9.04×10^{-12}	9.04×10^{-12}	2.10×10^{-05}	9.04×10^{-12}	9.04×10^{-12}	9.04×10^{-12}
	16	8.92×10^{-03}	2.95×10^{-11}	2.95×10^{-11}	2.62×10^{-09}	3.26×10^{-11}	2.95×10^{-11}	2.95×10^{-11}
Image 5	4	NaN	1.21×10^{-12}	1.21×10^{-12}	NaN	NaN	1.21×10^{-12}	NaN
	8	4.98×10^{-01}	1.76×10^{-11}	1.76×10^{-11}	2.68×10^{-02}	4.15×10^{-09}	1.76×10^{-11}	2.37×10^{-02}
	12	2.13×10^{-01}	2.20×10^{-11}	2.20×10^{-11}	1.51×10^{-03}	6.01×10^{-11}	2.20×10^{-11}	1.94×10^{-08}
	16	5.72×10^{-02}	2.86×10^{-11}	2.86×10^{-11}	4.00×10^{-09}	2.86×10^{-11}	2.86×10^{-11}	7.73×10^{-10}
Image 6	4	NaN	1.21×10^{-12}	1.21×10^{-12}	NaN	NaN	1.21×10^{-12}	NaN
	8	3.38×10^{-02}	2.82×10^{-11}	2.82×10^{-11}	3.03×10^{-04}	6.93×10^{-01}	2.82×10^{-11}	2.15×10^{-01}
	12	1.79×10^{-02}	3.00×10^{-11}	3.00×10^{-11}	9.02×10^{-08}	3.00×10^{-11}	3.00×10^{-11}	3.98×10^{-09}
	16	3.33×10^{-01}	3.02×10^{-11}	3.02×10^{-11}	3.01×10^{-07}	3.02×10^{-11}	3.02×10^{-11}	1.56×10^{-08}
Image 7	4	NaN	1.21×10^{-12}	1.21×10^{-12}	NaN	NaN	1.21×10^{-12}	NaN
	8	4.36×10^{-02}	8.87×10^{-12}	8.87×10^{-12}	4.91×10^{-02}	9.87×10^{-08}	8.87×10^{-12}	1.42×10^{-04}
	12	4.56×10^{-02}	2.22×10^{-11}	2.22×10^{-11}	5.89×10^{-04}	1.22×10^{-10}	2.22×10^{-11}	3.05×10^{-10}
	16	4.49×10^{-02}	2.96×10^{-11}	2.96×10^{-11}	2.06×10^{-08}	2.96×10^{-11}	2.96×10^{-11}	4.00×10^{-11}
Image 8	4	7.08×10^{-01}	5.14×10^{-12}	5.14×10^{-12}	1.78×10^{-02}	1.05×10^{-01}	5.14×10^{-12}	4.59×10^{-01}
	8	5.63×10^{-01}	2.94×10^{-11}	2.94×10^{-11}	6.64×10^{-02}	7.78×10^{-08}	2.94×10^{-11}	2.90×10^{-02}
	12	2.51×10^{-02}	3.01×10^{-11}	3.01×10^{-11}	8.88×10^{-10}	3.01×10^{-11}	3.01×10^{-11}	3.33×10^{-11}
	16	3.87×10^{-01}	3.02×10^{-11}	3.02×10^{-11}	8.15×10^{-11}	3.02×10^{-11}	3.02×10^{-11}	3.02×10^{-11}

Table A8. The CPU time for the MROA and comparison algorithms.

Image	nTh	MROA	ROA	RSA	AOA	AO	SSA	SCA	GWO
Image 1	4	1.8379	1.2774	0.7673	**0.5887**	1.1524	0.6932	0.6409	0.6846
	8	1.9090	1.2922	0.7895	0.5915	1.1807	0.7011	**0.5479**	0.6018
	12	2.1367	1.4243	0.9846	**0.6058**	1.1919	0.7098	0.6852	0.6668
	16	2.2943	1.5839	1.0903	**0.6425**	1.2171	0.7163	0.6630	0.7468
Image 2	4	1.8884	1.3400	0.7926	0.6556	1.1092	**0.6537**	0.6434	0.6246
	8	1.9155	1.2544	0.7368	0.6092	1.0052	0.6236	**0.5540**	0.6029
	12	2.1956	1.4925	0.8888	0.6844	1.1197	0.6210	**0.5861**	0.6386
	16	2.3795	1.5326	1.0408	0.6702	1.2512	**0.6586**	0.6819	0.6626
Image 3	4	1.8430	1.3069	0.7711	**0.5950**	1.1376	0.6922	0.6540	0.6255
	8	1.9125	1.3168	0.7436	**0.5538**	0.9963	0.6033	0.5804	0.6135
	12	2.1190	1.5218	0.8806	0.5997	1.1744	0.6486	**0.5827**	0.6043
	16	2.2936	1.5352	1.0334	0.7055	1.2035	0.7296	**0.6459**	0.6791

Table A8. *Cont.*

Image	nTh	MROA	ROA	RSA	AOA	AO	SSA	SCA	GWO
Image 4	4	1.8630	1.3688	0.7957	**0.6722**	1.1309	0.6726	0.6945	0.6642
	8	1.9396	1.3100	0.7478	0.5843	1.0390	0.5498	**0.5735**	0.6127
	12	2.1422	1.4025	0.9128	0.6430	1.0708	0.6095	**0.5939**	0.6114
	16	2.5628	1.5249	1.0577	0.7174	1.1687	**0.6639**	0.7192	0.6939
Image 5	4	1.8642	1.3274	0.8288	**0.6242**	1.1396	0.6730	0.6344	0.6666
	8	1.8793	1.3911	0.7755	0.5829	1.0591	**0.5451**	0.5688	0.5600
	12	2.1781	1.4372	0.9106	0.5894	1.0738	**0.5873**	0.5887	0.5966
	16	2.2633	1.5203	1.0575	**0.6301**	1.1780	0.6432	0.7161	0.6593
Image 6	4	1.8582	1.4131	0.8380	**0.6121**	1.1232	0.6806	0.6570	0.6517
	8	2.0519	1.2756	0.7370	0.5501	1.0023	0.6240	**0.5383**	0.5697
	12	2.1120	1.4508	0.8868	**0.5959**	1.1090	0.6999	0.5964	0.6241
	16	2.3020	1.5646	1.0270	0.6463	1.2760	0.7085	**0.6445**	0.6864
Image 7	4	1.8690	1.3777	0.7855	**0.6232**	1.1237	0.6944	0.6329	0.6491
	8	1.9270	1.3281	0.7436	0.5353	0.9974	0.5933	**0.5332**	0.5566
	12	2.1831	1.3844	0.8867	**0.5838**	1.0896	0.6509	0.5947	0.6173
	16	2.3213	1.5032	1.1525	**0.6419**	1.1959	0.7408	0.6577	0.6742
Image 8	4	1.8611	1.3340	0.7880	**0.6387**	1.1718	0.7102	0.6407	0.6419
	8	1.9048	1.3356	0.7345	**0.5370**	1.0652	0.5539	0.5455	0.5838
	12	2.1167	1.3882	0.8858	**0.5777**	1.1787	0.6169	0.5821	0.6676
	16	2.4502	1.5255	1.0484	**0.6479**	1.2839	0.7311	0.6500	0.6957

References

1. Bhandari, A.K. A novel beta differential evolution algorithm-based fast multilevel thresholding for color image segmentation. *Neural Comput. Appl.* **2020**, *32*, 4583–4613. [CrossRef]
2. He, L.; Huang, S. An efficient krill herd algorithm for color image multilevel thresholding segmentation problem. *Appl. Soft Comput.* **2020**, *89*, 106063. [CrossRef]
3. Bhandari, A.K.; Rahul, K. A novel local contrast fusion-based fuzzy model for color image multilevel thresholding using grasshopper optimization. *Appl. Soft Comput.* **2019**, *81*, 105515. [CrossRef]
4. Bhattacharyya, S.; Maulik, U.; Dutta, P. Multilevel image segmentation with adaptive image context based thresholding. *Appl. Soft Comput.* **2011**, *11*, 946–962. [CrossRef]
5. Anitha, J.; Pandian, I.A.; Agnes, S.A. An efficient multilevel color image thresholding based on modified whale optimization algorithm. *Expert Syst. Appl.* **2021**, *178*, 115003. [CrossRef]
6. Lei, B.; Fan, J. Multilevel minimum cross entropy thresholding: A comparative study. *Appl. Soft Comput.* **2020**, *96*, 106588. [CrossRef]
7. Lin, S.; Jia, H.; Abualigah, L.; Altalhi, M. Enhanced slime mould algorithm for multilevel thresholding image segmentation using entropy measures. *Entropy* **2021**, *23*, 1700. [CrossRef]
8. Kotte, S.; Pullakura, R.K.; Injeti, S.K. Optimal multilevel thresholding selection for brain MRI image segmentation based on adaptive wind driven optimization. *Measurement* **2018**, *130*, 340–361. [CrossRef]
9. Houssein, E.H.; Emam, M.M.; Ali, A.A. An efficient multilevel thresholding segmentation method for thermography breast cancer imaging based on improved chimp optimization algorithm. *Expert Syst. Appl.* **2021**, *185*, 115651. [CrossRef]
10. Zhou, Y.; Yang, X.; Ling, Y.; Zhang, J. Meta-heuristic moth swarm algorithm for multilevel thresholding image segmentation. *Multimed. Tools Appl.* **2018**, *77*, 23699–23727. [CrossRef]
11. Jiang, Y.; Yeh, W.; Hao, Z.; Yang, Z. A cooperative honey bee mating algorithm and its application in multi-threshold image segmentation. *Inform. Sci.* **2016**, *369*, 171–183. [CrossRef]
12. Sarkar, S.; Das, S. Multilevel Image Thresholding Based on 2D Histogram and Maximum Tsallis Entropy—A Differential Evolution Approach. *IEEE Trans. Image Process* **2013**, *22*, 4788–4797. [CrossRef] [PubMed]
13. Ahmadi, M.; Kazemi, K.; Aarabi, A.; Niknam, T.; Helfroush, M.S. Image segmentation using multilevel thresholding based on modified bird mating optimization. *Multimed. Tools Appl.* **2017**, *78*, 23003–23027. [CrossRef]
14. Abualigah, L.; Diabat, A.; Sumari, P.; Gandomi, A.H. A novel evolutionary arithmetic optimization algorithm for multilevel thresholding segmentation of COVID-19 CT images. *Processes* **2021**, *9*, 1155. [CrossRef]
15. Chen, H.; Li, W.; Yang, X. A whale optimization algorithm with chaos mechanism based on quasi-opposition for global optimization problems. *Expert Syst. Appl.* **2020**, *158*, 113612. [CrossRef]
16. Rao, R.V.; Vakharia, D.P. Teaching-learning-based optimization: A novel method for constrained mechanical design optimization problems. *Comput. Aided Des.* **2011**, *43*, 303–315. [CrossRef]

17. Wang, S.; Liu, Q.; Liu, Y.; Jia, H.; Abualigah, L.; Zheng, R.; Wu, D. A hybrid SSA and SMA with mutation opposition-based learning for constrained engineering problems. *Comput. Intell. Neurosci.* **2021**, *2021*, 6379469. [CrossRef]
18. Dinkar, S.K.; Deep, K.; Mirjalili, S.; Thapliyal, S. Opposition-based Laplacian Equilibrium Optimizer with application in image segmentation using multilevel thresholding. *Expert Syst. Appl.* **2021**, *174*, 114766. [CrossRef]
19. Zheng, R.; Jia, H.; Abualigah, L.; Liu, Q.; Wang, S. Deep ensemble of slime mold algorithm and arithmetic optimization algorithm for global optimization. *Processes* **2021**, *9*, 1774. [CrossRef]
20. Wang, S.; Jia, H.; Liu, Q.; Zheng, R. An improved hybrid aquila optimizer and harris hawks optimization for global optimization. *Math. Biosci. Eng.* **2021**, *18*, 7076–7109. [CrossRef]
21. Houssein, E.H.; Mahdy, M.A.; Blondin, M.J.; Shebl, D.; Mohamed, W.M. Hybrid slime mould algorithm with adaptive guided differential evolution algorithm for combinatorial and global optimization problems. *Expert Syst. Appl.* **2021**, *174*, 114689. [CrossRef]
22. Zheng, R.; Jia, H.; Abualigah, L.; Liu, Q.; Wang, S. An improved arithmetic optimization algorithm with forced switching mechanism for global optimization problems. *Math. Biosci. Eng.* **2021**, *19*, 473–512. [CrossRef] [PubMed]
23. Wang, S.; Jia, H.; Abualigah, L.; Liu, Q.; Zheng, R. An improved hybrid aquila optimizer and harris hawks algorithm for solving industrial engineering optimization problems. *Processes* **2021**, *9*, 1551. [CrossRef]
24. Li, Y.; Zhao, Y.; Liu, J. Dynamic sine cosine algorithm for large-scale global optimization problems. *Expert Syst. Appl.* **2021**, *177*, 114950. [CrossRef]
25. Zhang, Z.; Ding, S.; Jia, W. A hybrid optimization algorithm based on cuckoo search and differential evolution for solving constrained engineering problems. *Eng. Appl. Artif. Intel.* **2019**, *85*, 254–268. [CrossRef]
26. Khare, A.; Rangnekar, S. A review of particle swarm optimization and its applications in solar photovoltaic system. *Appl. Soft Comput.* **2013**, *13*, 2997–3006. [CrossRef]
27. Mirjalili, S.; Mirjalili, S.M.; Lewis, A. Grey wolf optimizer. *Adv. Eng. Softw.* **2014**, *69*, 46–61. [CrossRef]
28. Li, S.; Chen, H.; Wang, M.; Heidari, A.A.; Mirjalili, S. Slime mould algorithm: A new method for stochastic optimization. *Future Gener. Comput. Syst.* **2020**, *111*, 300–323. [CrossRef]
29. Mirjalili, S.; Lewis, A. The whale optimization algorithm. *Adv. Eng. Softw.* **2016**, *95*, 51–67. [CrossRef]
30. Abdel-Basset, M.; Hessin, A.N.; Abdel-Fatah, L. A comprehensive study of cuckoo-inspired algorithms. *Neural Comput. Appl.* **2018**, *29*, 345–361. [CrossRef]
31. Mirjalili, S.; Gandomi, A.H.; Mirjalili, S.Z.; Saremi, S.; Faris, H.; Mirjalili, S.M. Salp swarm algorithm: A bio-inspired optimizer for engineering design problems. *Adv. Eng. Softw.* **2017**, *114*, 163–191. [CrossRef]
32. Dorigo, M.; Birattari, M.; Stutzle, T. Ant colony optimization. *IEEE Comput. Intell. Mag.* **2006**, *1*, 28–39. [CrossRef]
33. Heidari, A.A.; Mirjalili, S.; Faris, H.; Aljarah, I.; Mafarja, M.; Chen, H. Harris hawks optimization: Algorithm and applications. *Future Gener. Comput. Syst.* **2019**, *97*, 849–872. [CrossRef]
34. Mirjalili, S. Moth-flame optimization algorithm: A novel nature-inspired heuristic paradigm. *Knowl. Based Syst.* **2015**, *89*, 228–249. [CrossRef]
35. Abualigah, L.; Yousri, D.; Abd, E.M.; Ewees, A.A. Aquila optimizer: A novel meta-heuristic optimization algorithm. *Comput. Ind. Eng.* **2021**, *157*, 107250. [CrossRef]
36. Katoch, S.; Chauhan, S.S.; Kumar, V. A review on genetic algorithm: Past, present, and future. *Multimed. Tools Appl.* **2021**, *80*, 8091–8126. [CrossRef]
37. Rakshit, P.; Konar, A.; Das, S. Noisy evolutionary optimization algorithms—A comprehensive survey. *Swarm Evol. Comput.* **2017**, *33*, 18–45. [CrossRef]
38. Slowik, A.; Kwasnicka, H. Evolutionary algorithms and their applications to engineering problems. *Neural Comput. Appl.* **2020**, *32*, 12363–12379. [CrossRef]
39. Nguyen, S.; Mei, Y.; Zhang, M. Genetic programming for production scheduling: A survey with a unified framework. *Complex Intell. Syst.* **2017**, *3*, 41–66. [CrossRef]
40. Simon, D. Biogeography-based optimization. *IEEE Trans. Evol. Comput.* **2008**, *12*, 702–713. [CrossRef]
41. Hansen, N.; Ostermeier, A. Completely Derandomized Self-Adaptation in Evolution Strategies. *Evol. Comput.* **2001**, *9*, 159–195. [CrossRef]
42. Kirkpatrick, S.; Gelatt, C.D.; Vecchi, M.P. Optimization by simulated annealing. *Science* **1983**, *220*, 671–680. [CrossRef]
43. Rashedi, E.; Nezamabadi-pour, H.; Saryazdi, S. GSA: A gravitational search algorithm. *Inform. Sci.* **2009**, *179*, 2232–2248. [CrossRef]
44. Ahmadianfar, I.; Haddad, O.B.; Chu, X. Gradient-based optimizer: A new metaheuristic optimization algorithm. *Inform. Sci.* **2020**, *540*, 131–159. [CrossRef]
45. Mirjalili, S. SCA: A sine cosine algorithm for solving optimization problems. *Knowl. Based Syst.* **2016**, *96*, 120–133. [CrossRef]
46. Tanyildizi, E.; Demir, G. Golden sine algorithm: A novel math-inspired algorithm. Golden sine algorithm: A novel math-inspired algorithm. *Adv. Electr. Comput. Eng.* **2017**, *17*, 71–78. [CrossRef]
47. Abualigah, L.; Diabat, A.; Mirjalili, S.; Elaziz, A.E.; Gandomi, A.H. The arithmetic optimization algorithm. *Comput. Methods Appl. Mech. Eng.* **2021**, *376*, 113609. [CrossRef]
48. Neggaz, N.; Houssein, E.H.; Hussain, K. An efficient henry gas solubility optimization for feature selection. *Expert Syst. Appl.* **2020**, *152*, 113364. [CrossRef]

49. Sun, P.; Liu, H.; Zhang, Y.; Meng, Q.; Tu, L.; Zhao, J. An improved atom search optimization with dynamic opposite learning and heterogeneous comprehensive learning. *Appl. Soft Comput.* **2021**, *103*, 107140. [CrossRef]
50. Liu, Y.; Tian, P. A multi-start central force optimization for global optimization. *Appl. Soft Comput.* **2015**, *27*, 92–98. [CrossRef]
51. Mirjalili, S.; Mirjalili, S.M.; Hatamlou, A. Multi-verse optimizer: A nature-inspired algorithm for global optimization. *Neural. Comput. Appl.* **2015**, *27*, 495–513. [CrossRef]
52. Jia, H.; Peng, X.; Lang, C. Remora optimization algorithm. *Expert Syst. Appl.* **2021**, *185*, 115665. [CrossRef]
53. Zheng, R.; Jia, H.; Abualigah, L.; Wang, S.; Wu, D. An improved remora optimization algorithm with autonomous foraging mechanism for global optimization problems. *Math. Biosci. Eng.* **2022**, *19*, 3994–4037. [CrossRef]
54. Wolpert, D.H.; Macready, W.G. No free lunch theorems for optimization. *IEEE Trans. Evol. Comput.* **1997**, *1*, 67–82. [CrossRef]
55. Jia, H.; Lang, C.; Oliva, D.; Song, W.; Peng, X. Dynamic harris hawks optimization with mutation mechanism for satellite image segmentation. *Remote Sens.* **2019**, *11*, 1421. [CrossRef]
56. Ewees, A.A.; Abualigah, L.; Yousri, D.; Sahlol, A.T.; Al-qaness, A.A.; Alshathri, S.; Elaziz, M.A. Modified artificial ecosystem-based optimization for multilevel thresholding image segmentation. *Mathematics* **2021**, *9*, 2363. [CrossRef]
57. Houssein, E.H.; Hussain, K.; Abualigah, L.; Elaziz, M.A.; Alomoush, W.; Dhiman, G.; Djenouri, Y.; Cuevas, E. An improved opposition-based marine predators algorithms for global optimization and multilevel thresholding image segmentation. *Knowl.-Based Syst.* **2021**, *229*, 107348. [CrossRef]
58. Su, H.; Zhao, D.; Yu, F.; Heidari, A.A.; Zhang, Y.; Chen, H.; Li, C.; Pan, J.; Quan, S. Horizontal and vertical search artificial bee colony for image segmentation of COVID-19 X-ray images. *Comput. Biol. Med.* **2021**, *142*, 105181. [CrossRef]
59. Liu, L.; Zhao, D.; Yu, F.; Heidari, A.A.; Ru, J.; Chen, H.; Mafarja, M.; Turabieh, H.; Pan, Z. Performance optimization of differential evolution with slime mould algorithm for multilevel breast cancer image segmentation. *Comput. Biol. Med.* **2021**, *138*, 104910. [CrossRef]
60. Li, Y.; Bai, X.; Jiao, L.; Xue, Y. Partitioned-cooperative quantum-behaved particle swarm optimization based on multilevel thresholding applied to medical image segmentation. *Appl. Soft Comput.* **2017**, *56*, 345–356. [CrossRef]
61. Sun, K.; Jia, H.; Li, Y.; Jiang, Z. Hybrid improved slime mould algorithm with adaptive β hill climbing for numerical optimization. *J. Intell. Fuzzy Syst.* **2021**, *40*, 1667–1679. [CrossRef]
62. Faramarzi, A.; Heidarinejad, M.; Mirjalili, S.; Gandomi, A.H. Marine predators algorithm: A nature-inspired metaheuristic. *Expert Syst. Appl.* **2020**, *152*, 113377. [CrossRef]
63. Tizhoosh, H.R. Opposition-based learning: A new scheme for machine intelligence. In Proceedings of the Computational Intelligence for Modelling, Control & Automation, Vienna, Austria, 28–30 November 2005.
64. Chauhan, S.; Vashishtha, G.; Kumar, A. A symbiosis of arithmetic optimizer with slime mould algorithm for improving global optimization and conventional design problem. *J. Supercomput.* **2022**, *78*, 6234–6274. [CrossRef]
65. Kullback, S. *Information Theory and Statistics*; Dover: New York, NY, USA, 1968.
66. Oliva, D.; Hinojosa, S.; Cuevas, E.; Pajares, G.; Avalos, O.; Galvez, J. Cross entropy based thresholding for magnetic resonance brain images using Crow Search Algorithm. *Expert Syst. Appl.* **2017**, *79*, 164–180. [CrossRef]
67. Esparza, E.R.; Calzada, L.A.Z.; Oliva, D.; Heidari, A.A.; Zaldivar, D.; Cisneros, M.P.; Foong, L.K. An efficient harris hawks-inspired image segmentation method. *Expert Syst. Appl.* **2020**, *155*, 113428. [CrossRef]
68. Gill, H.S.; Khehra, B.S.; Singh, A.; Kaur, L. Teaching-learning-based optimization algorithm to minimize cross entropy for Selecting multilevel threshold values. *Egypt. Inform. J.* **2019**, *20*, 11–25. [CrossRef]
69. Abualigah, L.; Elaziz, M.A.; Sumari, P.; Geem, Z.; Gandomi, A.H. Reptile search algorithm (RSA): A nature-inspired meta-heuristic optimizer. *Expert Syst. Appl.* **2022**, *191*, 116158. [CrossRef]
70. Houssein, E.H.; Neggaz, N.; Hosney, M.E.; Mohamed, W.M.; Hassaballah, M. Enhanced Harris hawks optimization with genetic operators for selection chemical descriptors and compounds activities. *Neural Comput. Appl.* **2021**, *33*, 13601–13618. [CrossRef]
71. Bao, X.; Jia, H.; Lang, C. A Novel Hybrid Harris Hawks Optimization for Color Image Multilevel Thresholding Segmentation. *IEEE Access* **2019**, *7*, 76529–76546. [CrossRef]
72. Sara, U.; Akter, M.; Uddin, M.S. Image quality assessment through FSIM, SSIM, MSE and PSNR—A comparative study. *J. Comput. Commun.* **2019**, *7*, 8–18. [CrossRef]
73. Wang, Z.; Bovik, A.C.; Sheikh, H.R.; Simoncelli, E.P. Image quality assessment: From error visibility to structural similarity. *IEEE Trans. Image Process.* **2004**, *13*, 600–612. [CrossRef] [PubMed]
74. Jia, H.; Ma, J.; Song, W. Multilevel Thresholding Segmentation for Color Image Using Modified Moth-Flame Optimization. *IEEE Access* **2019**, *7*, 44097–44134. [CrossRef]
75. Xing, Z. An improved emperor penguin optimization based multilevel thresholding for color image segmentation. *Knowl. Based Syst.* **2020**, *194*, 105570. [CrossRef]